IN-82
417286

Smart Optical RAM for Fast Information Management and Analysis

submitted to

NASA Ames Research Center

by

Hua-Kuang Liu, Ph. D.

Principal Investigator

Professor of Electrical Engineering

University of South Alabama

Mobile, Alabama 36688

Tel. (334)460-7516, Fax. (334)460-6028

E-mail: liuhk@aol.com

November 23, 1998

TABLE OF CONTENTS

Smart Optical RAM for Fast Information Management and Analysis

I.   Project Overview

1.1   Statement of Problem

Instruments for high speed and high capacity in-situ data identification, classification and storage capabilities are needed by NASA for the information management and analysis of extremely large volume of data sets in future space exploration, space habitation and utilization, in addition to the various missions to planet-earth programs. Parameters such as communication delays, limited resources, and inaccessibility of human manipulation require more intelligent, compact, low power, and light weight information management and data storage techniques. New and innovative algorithms and architecture using photonics will enable us to meet these challenges. The technology has applications for other government and public agencies.

1.2   Solution of the Problem

In this NASA Advanced Concept Fellow Program, we have proposed and investigated a totally new and innovative optical random-access memory (RAM) system. Comparing to the digital RAM in electronic computers, the optical RAM has much broader capabilities. The optical RAM can be used not only for the storage of an extremely large amount of information and fast random-access to the data but also for pattern classification and interconnections in future advanced computers.
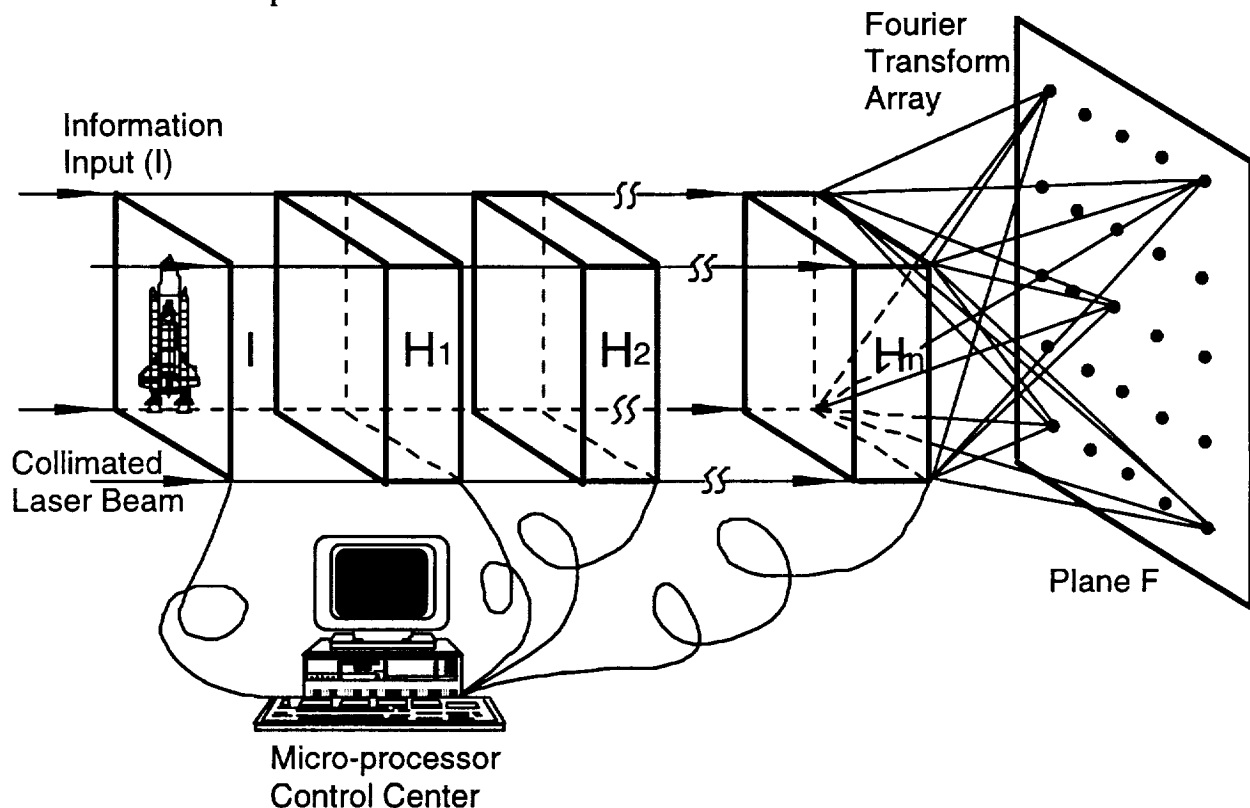

Figure 1   An optical random-access memory (RAM) system block diagram.

2

The new optical RAM is conceptually illustrated in Fig. 1. The information input I in a 2-D image or data format is carried by a collimated laser beam and applied through a sequence of multiple stages of cascaded holographic optical elements (HOE) and shutter arrays denoted by the H blocks. The HOE in H_1 will divide and replicate the input I into an array of $h_1 x h_1$ identical images. The shutter array in H_1 is electronically controlled which can let any of the $(h_1)^2$ replica of I passing through the optical system. The subsequent H blocks have similar functions and capabilities. Hence at the output of the block H_n, $(h_1 h_2 .... h_n)^2$ replica of I will appear in a Fourier transform array at plane F. For example, if 2 stages of H are used with $h_1=9$ and $h_2=5$, $(45)^2= 2,025$ Fourier transforms of I can be obtained at plane F. If 4 stages of H are used with $h_1=h_3=9$ and $h_2=h_4=5$, $(9x5x9x5)^2=4,100,625$ Fourier transforms of I can be stored at plane F. If the input data are people's faces, then all the faces of any one of most of the cities in the world can be memorized in the optical RAM. Furthermore, random accessible retrieval can be achieved at the speed of light! The memory can be accessed by simultaneous switching the shutter arrays.

1.3   Potential Applications

In contrast to the conventional optical correlators that can process only one channel at a given instant, the proposed optical RAM can memorize tens of thousands of channels of 2-D information of on the order of megabytes and retrieve information accurately at the speed of light. Partial information input can recall complete information from the optical RAM. These unique abilities of the optical RAM allow it to be applied to many current fields of interest, including parallel database search, image and signal understanding and synthesis, real-time multi-sensory target recognition and classification, and parallel optical interconnections for future computers. These areas are of importance to NASA's future space exploration, space habitation and utilization, in addition to the various missions to planet-earth programs and many commercial applications including fingerprints identification for police and FBI and optical interconnections for future computers.

For purpose of demonstration, one example of these applications is illustrated in Fig. 2. Fig. 2(a) shows how memorization in the optical RAM is accomplished by placing the objects as represented by the satellite and space shuttle in the view of a video camera. Over tens of thousands of 2-D data can be stored. Microprocessors may be used to control the random access to any data set from the memory. After the optical RAM memorizes all the images presented to it, it becomes smart. When input such as a partial and noisy space shuttle as shown in Fig. 2(b), is presented to it, the smart RAM can recover and display at the output screen the perfectly retrieved image. In addition, the optical RAM can be used to recognize input and tells us whether it belongs to the memory. For example, if the fingerprints of FBI's most wanted criminals are stored in the memory, the RAM can determine whether an arbitrary input fingerprint belongs to one of the criminals. This can be done remotely and the optical RAM can make decision at the speed of light!

In summary, a few potential NASA and commercial applications are summarized below:

NASA Applications

   a)   Planetary exploration in-situ data analysis and information screening
   b)   Space surveillance specific object identification and navigation guidance
   c)   Space image understanding and classification
   d)   Space station automated rendezvous and docking
   e)   Space habitation and utilization environmental evaluation and assessment
   f)   Navigation collision avoidance in Moon and Mars
   g)   Satellite repair, maintenance and sensing

Commercial applications

   a)   Criminal fingerprints random access memory and retrieval for police
   b)   Security check of commercial building entrances
   c)   Automobile plate identification
   d)   Large capacity free space interconnection for future computers
   e)   Border patrol and illegal drug traffic prevention

1.4   Innovation of the Work

Comparing with existing technology can show the innovation. For example, the operation of a digital computer requires that data can be stored and retrieved as desired, and information can be put randomly into and out of each storage element as required. A digital RAM is used for this purpose. However, according to Professor Jacob Millman of Columbia University, a major disadvantage of the digital RAM is that it is volatile. Due to the fact that dynamic circuits are exclusively used for large storage capacity, stored information is lost when the power is turned off. The proposed optical RAM has some functions of a digital RAM but is non-volatile. When the laser light is turned off, the memory remains in the hologram. Similar optical technology for memory are limited to single channel operation with limited data throughput data processing capacity, the proposed optical RAM has good sensitivity, high resolution, speed-of-light photon processing, massive parallelism, accurate smart retrieval, and real-time operation capability.

1.5   Concept Impact

The optical RAM, which is quite different from the electronic RAM, displays a higher level capability of optical multiplexing a 2D input and comparing it with many different reference data sets, and can create an oscillatory optical resonance mode in which input variation and error can be eliminated. As erasable optical recording materials such as the thermoplastic material and photorefractive materials are used, the information will remain in the memory until the writing of new information into the system. In addition to the conventional memory capability similar to a digital RAM, it has the added capability of parallel pattern classification for information management that the digital RAM does not have.   For NASA, the impact of the concept on increased automation and increased efficiency in information management based on the optical RAM means that previously impossible missions are enabled.
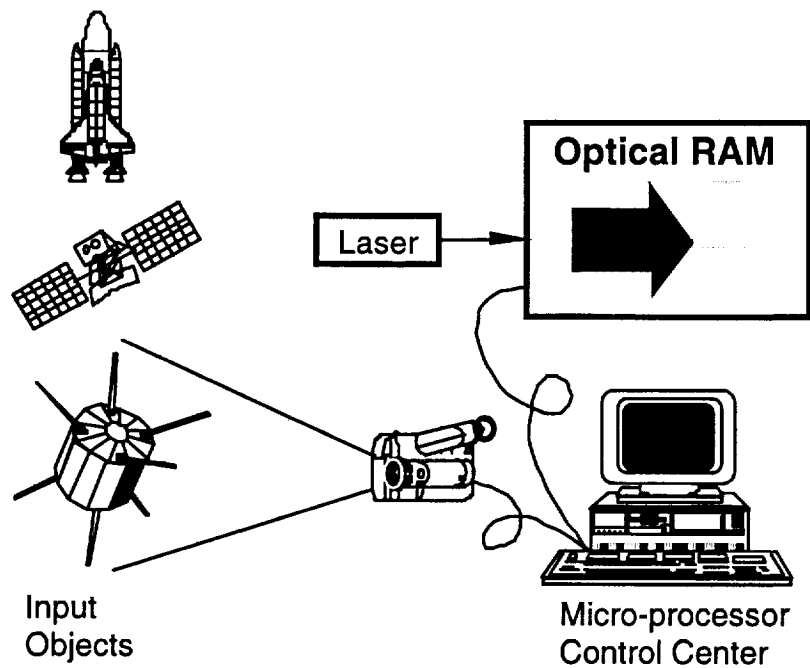
(a)
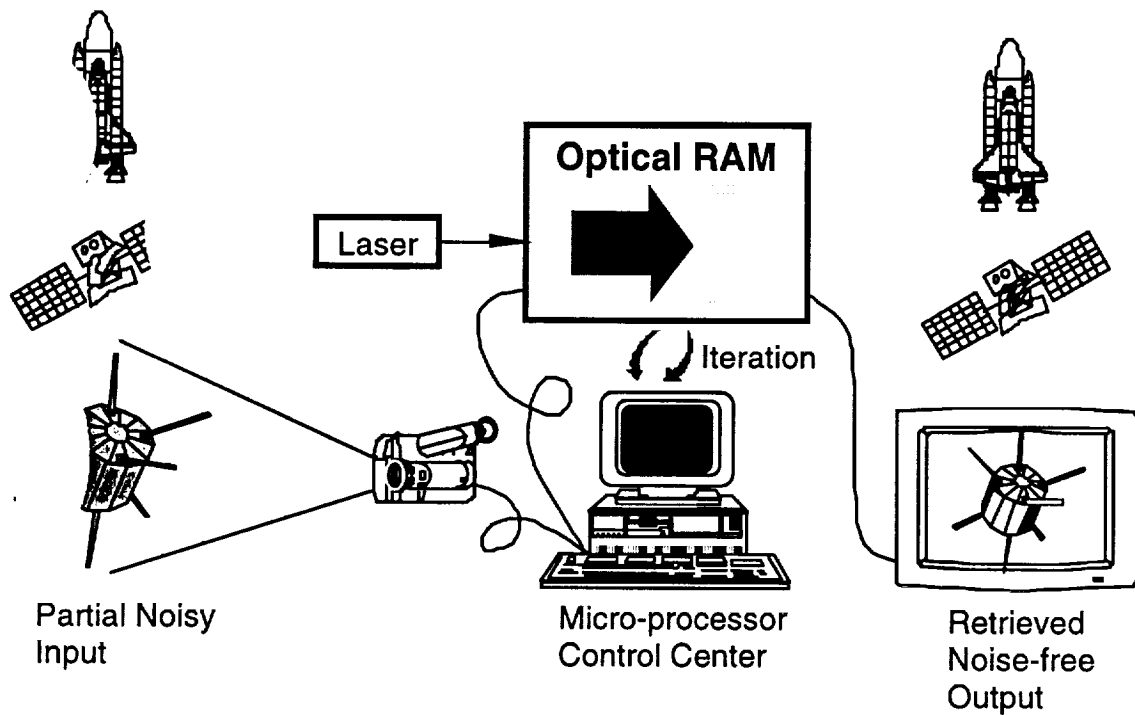
(b)

Figure 2.   Example of the applications of an optical RAM. (a) Memory process; (b) Information retrieval.

II. Description of the Project

2.1 Project Objective

For the purpose of serving future NASA space exploration, space habitation and utilization, in addition to the various missions to planet-earth programs, we have investigated a new and innovative optical random-access memory (RAM) with high data throughput parallel free space optical holographic interconnection and memory capabilities for fast information management and analysis.

2.2 Theoretical Background

To further illustrate the concept as shown in Fig. 3, multi-channel pattern recognition architecture utilizing a cascade combination of a Dammann grating and a holographic lens is shown in Fig. 4. A laser beam from an Argon ion laser is divided into two beams, an object beam and a reference beam, by a beam splitter. The object beam is collimated by a spatial filter and lens L_1 combination and is replicated by a Dammann grating into a (2M+1) x (2M+1) array of beams, where M is the maximum diffraction order of the Dammann grating. The object beam array illuminate the input pattern and are then Fourier transformed by the lens L_2 at its focal plane where selection shutter array 1 is placed. The input pattern array can be Fourier transformed by lens L_3 and be replicated into a (2N+1) x (2N+1) array, where N is maximum order of the holographic lens, and Fourier transformed again by the holographic lens at its focal plane where selection shutter array 2 is placed. The lenses L_4 and L_5 are used to perform the Fourier transform to yield the $(2M+1)^2$ x $(2N+1)^2$ array at the L_5 focal plane as shown in Fig. 3 where the holographic matched filter is recorded. The reference beam is collimated by a spatial filter and lens L combination and interferes with the object beam at the matched filter plane.

A theoretical analysis of the multi-channel system in Fig. 3 is described below.

A. Amplitude distribution at plane P_2 (Fourier plane of L_2)

The object is illumined by an array of beams diffracted by the Dammann grating and is Fourier transformed by lens L_2 onto its Fourier plane P_2 where an aperture is set to select only (2M+1) x (2M+1) equally bright central diffraction orders. The amplitude distribution at P_2 is a (2M+1) x (2M+1) array of Fourier transforms of the object by lens L_2

$$S_2(f_x, f_y) = \frac{A}{j\lambda f_2} \sum_{m_d=-M}^{M} \sum_{n_d=-M}^{M} \delta(f_x - \frac{m_d}{L_d})\delta(f_y - \frac{n_d}{L_d}) * F_2\{O(x,y)\}$$

$$= \frac{A}{j\lambda f_2} \sum_{m_d=-M}^{M} \sum_{n_d=-M}^{M} \delta(f_x - \frac{m_d}{L_d})\delta(f_y - \frac{n_d}{L_d}) * \tilde{O}(f_x, f_y)$$
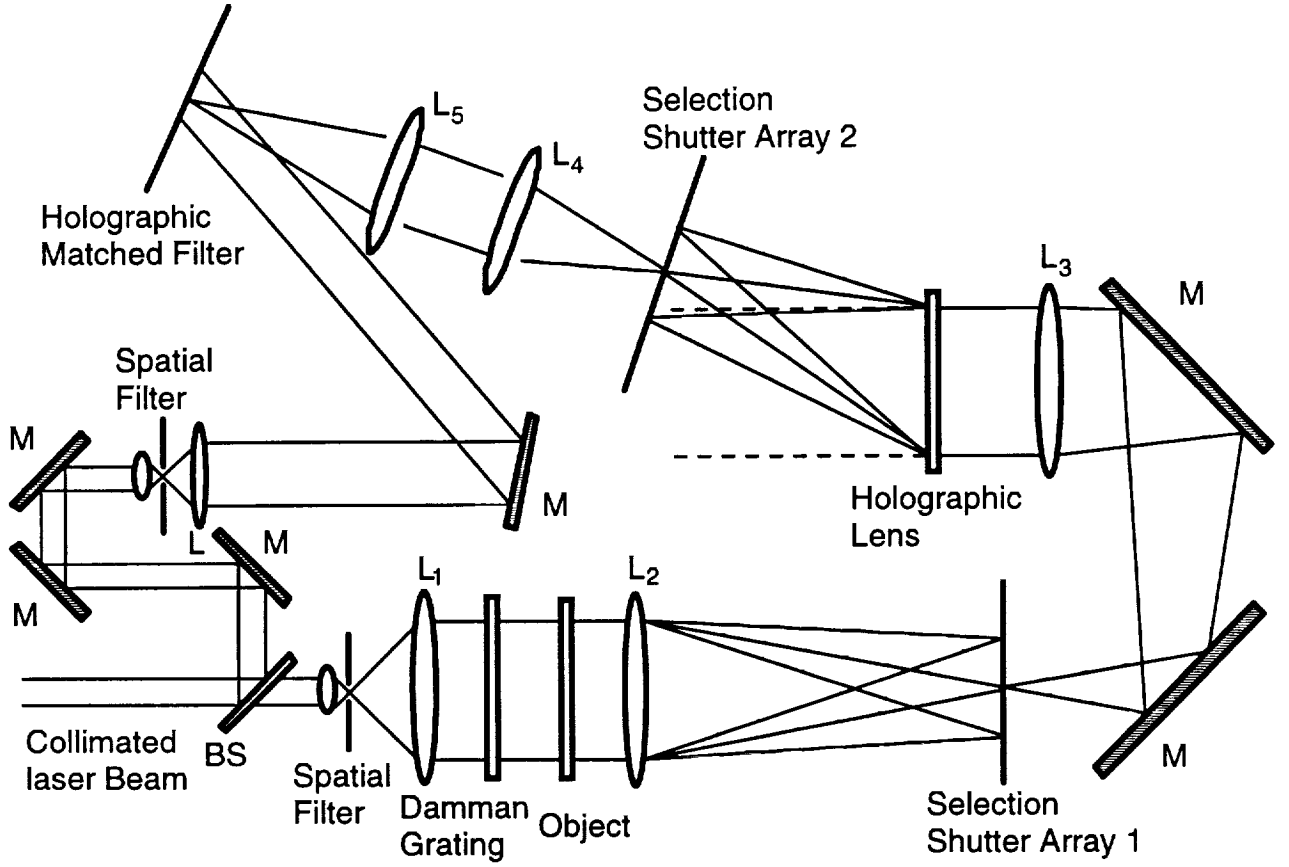
(1)

6

Figure 3   The experimental setup of a multi-channel pattern recognition architecture
            utilizing a cascade combination of a Dammann Grating and a holographic
            lens.

where l is the wavelength of the laser, A is a constant associated with the input wave amplitude, f_2 is the focal length of lens L_2, and $1/L_d$ is the periodic of the Dammann Grating in frequency domain. $F_n\{\}$ denotes the Fourier transform by lens L_n (n=1, 2, ...),

$$\bar{O}(f_x, f_y) = F_2\{O(x, y)\} = \iint O(x, y) exp[-j2\pi(f_x x + f_y y)]dxdy \qquad (2)$$

where f_x and f_y are the special frequencies: $f_x = x_2/(lf_2)$ and $f_y = y_2/(lf_2)$, and (x_2, y_2) are points in plane P_2. The amplitude distribution at P_2 can also be expressed in terms of the position at plane P_2

$$U_2(x_2, y_2) = S_2(\frac{x_2}{\lambda f_2}, \frac{y_2}{\lambda f_2})$$

$$= \frac{A}{j(\lambda f_2)^3} \sum_{m_d=-M}^{M} \sum_{n_d=-M}^{M} \delta(x_2 - \frac{\lambda f_2}{L_d} m_d) \delta(y_2 - \frac{\lambda f_2}{L_d} n_d) * \bar{O}(\frac{x_2}{\lambda f_2}, \frac{y_2}{\lambda f_2})$$ (3)

$$= \frac{A}{j\lambda f_2} M_d(x_2, y_2) * \bar{O}(\frac{x_2}{\lambda f_2}, \frac{y_2}{\lambda f_2})$$

Where

$$M_d(x_2, y_2) = \frac{1}{(\lambda f_2)^2} \sum_{m_d=-M}^{M} \sum_{n_d=-M}^{M} \delta(x_2 - \frac{\lambda f_2}{L_d} m_d) \delta(y_2 - \frac{\lambda f_2}{L_d} n_d)$$ (4)

B. Amplitude distribution at Fourier plane of lens L_3

A lens L_3 is placed at distance f_3 from plane P_2. Due to the input at plane P_2, the amplitude distribution at Fourier plane of lens L_3 may be written as

$$S_3(f_{x2}, f_{y2}) = \frac{1}{j\lambda f_3} F_3\{U_2(x_2, y_2)\}$$

$$= -\frac{A}{(\lambda f_2)(\lambda f_3)} F_3\{M_d(x_2, y_2)\} \cdot F_3 F_2\{O(x, y)\}$$ (5)

The amplitude distribution Eq. (5) can also be expressed in terms of the position at Fourier plane of lens L_3, that is

$$U_3(x_3, y_3) = S_3(\frac{x_3}{\lambda f_3}, \frac{y_3}{\lambda f_3})$$

$$= -\frac{A}{(\lambda f_2)(\lambda f_3)} \bar{M}_d(\frac{x_3}{\lambda f_3}, \frac{y_3}{\lambda f_3}) \cdot O(-\frac{f_2}{f_3} x_3, -\frac{f_2}{f_3} y_3)$$ (6)

where $\bar{M}_d(f_x, f_y) = F_3\{M_d(x, y)\}$.

C. Amplitude distribution at Fourier plane of the holographic lens

The holographic lens Fourier transforms the input $U_3(x_3, y_3)$ to a (2N+1) x (2N+1) array of spectrum onto its Fourier transform plane. The amplitude distribution is

8

$$S_h(f_{x3}, f_{y3}) = \frac{1}{j\lambda f_h} \sum_{m_h=-N}^{N} \sum_{n_h=-N}^{N} \delta(f_{x3} - \frac{m_h}{L_h})\delta(f_{y3} - \frac{n_h}{L_h}) * F_h\{U_3(x_3, y_3)\}$$

$$= -\frac{A}{j(\lambda f_2)(\lambda f_3)(\lambda f_h)} \sum_{m_h=-N}^{N} \sum_{n_h=-N}^{N} \delta(f_{x3} - \frac{m_h}{L_h})\delta(f_{y3} - \frac{n_h}{L_h})$$

$$* F_h F_3\{M_d(x_2, y_2)\} * F_h\{O(-\frac{f_2}{f_3}x_3, -\frac{f_2}{f_3}y_3)\}$$

$$= -\frac{A}{j(\lambda f_2)(\lambda f_3)(\lambda f_h)} \sum_{m_h=-N}^{N} \sum_{n_h=-N}^{N} \delta(f_{x3} - \frac{m_h}{L_h})\delta(f_{y3} - \frac{n_h}{L_h})$$

$$* F_h F_3\{M_d(x_2, y_2)\} * F_h F_3\{\bar{O}(\frac{x_2}{\lambda f_2}, \frac{y_2}{\lambda f_2})\}$$

(7)

The amplitude distribution Eq. (7) can also be expressed in terms of the position at Fourier plane of the holographic lens, that is

$$U_h(x_h, y_h) = S_3(\frac{x_h}{\lambda f_h}, \frac{y_h}{\lambda f_h})$$

$$= -\frac{A}{j(\lambda f_2)(\lambda f_3)(\lambda f_h)} \frac{1}{(\lambda f_h)^2} \sum_{m_h=-N}^{N} \sum_{n_h=-N}^{N} \delta(x_h - \frac{\lambda f_h}{L_h}m_h)\delta(y_h - \frac{\lambda f_h}{L_h}n_h)$$

$$* M_d(-\frac{f_3}{f_h}x_h, -\frac{f_3}{f_h}y_h) * \bar{O}(-\frac{f_3}{\lambda f_2 f_h}x_h, -\frac{f_3}{\lambda f_2 f_h}y_h)$$

(8)

$$= -\frac{A}{j(\lambda f_2)(\lambda f_3)(\lambda f_h)} M_h(x_h, y_h) * M_d(-\frac{f_3}{f_h}x_h, -\frac{f_3}{f_h}y_h) * \bar{O}(-\frac{f_3}{\lambda f_2 f_h}x_h, -\frac{f_3}{\lambda f_2 f_h}y_h)$$

where f_h is the focal length of the holographic lens, $1/L_h$ is the periodic of the holographic lens in frequency domain, and

$$M_h(x_h, y_h) = \frac{1}{(\lambda f_h)^2} \sum_{m_h=-N}^{N} \sum_{n_h=-N}^{N} \delta(x_h - \frac{\lambda f_h}{L_h}m_h)\delta(y_h - \frac{\lambda f_h}{L_h}n_h)$$

(9)

D.   Amplitude distribution at Matched filter Plane

L_4 and L_5 are a pair of lenses with same focal length. Lens L_4 is placed at distance $f_4 = f_5$ from the Fourier plane of the holographic lens and lens L_5 is placed $2f_4$ from lens L_4. The matched filter plane is at the focal plane of lens L_5. The amplitude distribution at matched filter plane can be expressed as

$$U_m(x_m, y_m) = -\frac{1}{\lambda^2 f_4^2} F_5 F_4\{U_h(x_h, y_h)\}$$

(10)

since $f_4 = f_5$, then

$$U_m(x_m, y_m) = -\frac{1}{\lambda^2 f_4^2} U_h(-x_m, -y_m)$$

$$= \frac{A}{j(\lambda f_2)(\lambda f_3)(\lambda f_h)(\lambda f_4)^2} M_h(-x_m, -y_m) * M_d(\frac{f_3}{f_h} x_m, \frac{f_3}{f_h} y_m) * \bar{O}(\frac{f_3}{\lambda f_2 f_h} x_m, \frac{f_3}{\lambda f_2 f_h} y_m) \quad (11)$$

where (x_m, y_m) is the position at matched filter plane. It can be seen that the amplitude distribution at the matched filter plane is a (N x N) with (M x M) array of the Fourier transforms of the object

$$\bar{O}(f_x, f_y) = F_2\{O(x, y)\} = \iint O(x, y) exp[-j2\pi(f_x x + f_y y)] dx dy$$

with

$$f_x = \frac{f_3}{\lambda f_2 f_h} x_m \text{ and } f_y = \frac{f_3}{\lambda f_2 f_h} y_m$$

E. Recording of the Holographic Matched filter

In the recording of the holographic matched filter, two selection arrays are placed at the plane P$_2$ and at the Fourier plane of the holographic lens, respectively. The selection arrays are set that only one order from the Dammann grating or the holographic lens is selected to go through while other orders are blocked. Once the order (m_1, n_1) from Dammann grating and the order (m_2, n_2) from holographic lens are selected, the amplitude distribution at the matched filter plane, or Eq. (11), becomes

$$U_m(x_m, y_m) = \frac{A}{j(\lambda f_2)^3 (\lambda f_3)(\lambda f_h)^3 (\lambda f_4)^2} \delta(-x_m - \frac{\lambda f_h}{L_h} m_2) \delta(-y_m - \frac{\lambda f_h}{L_h} n_2)$$

$$* \delta(\frac{f_3}{f_h} x_m - \frac{\lambda f_2}{L_d} m_1) \delta(\frac{f_3}{f_h} y_m - \frac{\lambda f_2}{L_d} n_1) * \bar{O}(\frac{f_3}{\lambda f_2 f_h} x_m, \frac{f_3}{\lambda f_2 f_h} y_m)$$

$$= \frac{A \lambda f_3}{j(\lambda f_2)^3 (\lambda f_h)^5 (\lambda f_4)^2} \delta(-x_m - \frac{\lambda f_h}{L_h} m_2) \delta(-y_m - \frac{\lambda f_h}{L_h} n_2) \quad (12)$$

$$* \delta(x_m - \frac{\lambda f_2 f_h}{f_3 L_d} m_1) \delta(y_m - \frac{\lambda f_2 f_h}{f_3 L_d} n_1) * \bar{O}(\frac{f_3}{\lambda f_2 f_h} x_m, \frac{f_3}{\lambda f_2 f_h} y_m)$$

2.3 Research Results

The latest results of the research are included in the preprint of a manuscript as shown below. Other results including papers published and patent application are included in the appendixes.

Massively parallel optical pattern recognition and retrieval via a two-stage high-capacity multi-channel holographic random-access memory system

Luzhong Cai*

Hua-Kuang Liu, FELLOW SPIE

University of South Alabama

Department of Electrical and Computer Engineering

Mobile, Alabama 36688

E-mail: lcai@usamail.usouthal.edu

*Permanent address: Shandong University, Department of Optics, Jinan, 250100, China

11

Abstract. The multi-stage holographic optical random-access memory (HORAM) system reported recently by Liu et al provides a new degree of freedom for improving the storage capacity. In this paper we further presented theoretical and practical analysis on the HORAM system with experimental results. Our discussions included the system design and geometrical requirements, its applications for multi-channel pattern recognition and associate memory, the 2-D and 3-D information storage capacity, and the multi-channel image storage and retrieval via Vander Lugt correlator (VLC) filters and joint transform holograms. A series of experiments have been performed to demonstrate the feasibility of the multi-channel pattern recognition and image retrieval with both of the VLC and joint transform correlator (JTC) architectures. The experimental results with as many as 2025 channels have shown good agreement with the theoretical analysis.

Subject terms: multi-stage holographic optical random-access memory system; holographic storage; optical pattern recognition; image storage and retrieval; optical information processing.

12

1 Introduction

Optical data storage and pattern recognition are two important and related areas in modern optics. For the purpose of optical pattern recognition, a variety of architectures and techniques have been developed, which are mainly categorized into Vander Lugt correlator (VLC)[1-4] and joint transform correlator (JTC)[5-8] systems. Optical data storage offers inherent 2-D parallelism and high speed processing. It may enable one to construct a holographic database with a large number of image templates optically accessible and applicable for different applications including pattern recognition, image retrieval, and associate memory. In order to increase the image storage and recognition capability of a system, several methods have been proposed and experimentally demonstrated. These include the composite filter synthesis[9-10] and multiplexing techniques with the use of a volume recording element[11-20]. The latter approach has been considered as one of the most successful and promising techniques for data storage. For example, Heanue et al demonstrated the storage and retrieval of digital data using a volume hologram[12], Mok reported that over thousands of holograms can be stored in a lithium niobate crystal via angular multiplexing[13], and Pu et al reported the storage of up to one thousand holograms at a single location using the DuPont 100-μm-thick photopolymer[20]. In these techniques, either the volume effect of a 3-D recording device or the one-stage spectrum multiplexing is used to enhance the storage capacity of a given system. More recently, Liu et al presented a multi-stage holographic optical random-access memory (HORAM) system[21,22], which has advantages including higher storage capacity over a single stage system.

In this paper we will discuss the design principles of the multi-stage HORAM system for its practical applications. We will introduce a few architectures for different applications and, for the first time, present new and more detailed experimental demonstration results of multi-channel

pattern recognition and reconstruction with the use of a two-stage HORAM system including VLC and JTC arrangements. The results have verified the feasibility and usefulness of a multi-stage multi-channel HORAM system.

2 Theoretical analyses

2.1 *Geometrical considerations for spectrum array generation and separation*

A multi-stage HORAM system is composed of several stages cascaded in tandem. The use of many stages in a system can greatly increase the spectrum multiplexing capacity, but it also introduces the complication in the interconnection between any two succeeding stages. In order to ensure that all the spectra of different orders in the final spatial spectrum plane are properly separated, the optical arrangement of a HORAM system should satisfy certain geometrical requirements. In the following we will discuss these requirements for a two-stage HORAM system.

The working principle of a two-stage HORAM system may be schematically expressed in Fig.1, where (a), (b) and (c) are the optical setup and the spectral distributions in planes F and H, respectively. The light from a point coherent source, S, becomes a plane wave after passing through collimator L_1, and then illuminates the object transparency, O, which is in close contact with a Dammann grating, G. The first spectrum array is obtained at the back focal plane F of lens L_2. The grating G may produce many diffraction orders in plane F. By inserting a rectangular opening aperture we can select only M×M central diffraction orders and block the higher orders. A combination of lens L_3 and a multi-focus hololens, L_h, images plane F onto plane H. In plane H the spectrum is further multiplexed to a (M×M)×(N×N) array, where the N×N multiplexing is produced by the hololens.

If we assume the Dammann grating has the same spatial frequency v_d in the x and y directions, the length of one side of the M×M spectrum array in plane F can be decided by

$$D_f = D_x = D_y = M\lambda f_2 v_d , \qquad (1)$$

where λ is the wavelength of the laser, and f_2 is the focal length of lens L_2. This pattern is magnified in plane H by a factor

$$A = \frac{f_h}{f_3} , \qquad (2)$$

and the hololens L_h further replicates the magnified M × M spectrum array to N × N arrays with a spacing

$$D_h = \lambda v_h f_h, \qquad (3)$$

where f_3 and f_h are the focal lengths of L_3 and L_h, respectively, and v_h is the spatial frequency of the hololens. Obviously, in order to separate different orders in plane H, we need

$$D_h \geq AD_f , \qquad (4)$$

that is

$$v_h \geq M \frac{f_2}{f_3} v_d , \qquad (5)$$

or, if we use the parameter A,

$$A \leq \frac{f_h v_h}{M f_2 v_d} . \qquad (6)$$

Actually the planes F and H are not necessarily placed in the front focal plane of L_3 and back focal plane of L_h, respectively. What we need here is the multiple imaging function, which can be performed by either a single multi-focus hololens or a combination of a multi-focus hololens

and another conventional lens, as shown in Fig.2 (a) and (b). In both cases the magnification from F to H may be written

$$A = \frac{d_h}{d_f}.$$ (7)

The requirements similar to Eqs. (5) and (6) may then be written as

$$v_h \geq M \frac{f_2}{d_f} v_d$$ (8)

and

$$A \leq \frac{d_h v_h}{M f_2 v_d},$$ (9)

or equivalently

$$d_f \geq \frac{M f_2 v_d}{v_h}.$$ (10)

We can see that the changes here are the substitutions of f_3 and f_h by d_f and d_h, respectively. We may use Eq. (10) to adjust the magnification of the imaging system to ensure spectrum separation. In the exact matching case where the equal sign is used in all the above expressions, we will obtain an equal spacing $(N \times N) \times (M \times M)$ spectrum array in plane H.

The size of the $M \times M$ spectrum array in plane F has been given in Eq. (1). In case of exact matching, the $(N \times N) \times (M \times M)$ spectrum array in H has the size $D \times D$, where

$$D = N \frac{d_h}{d_f} D_f = MN \lambda f_2 v_d \frac{d_h}{d_f}.$$ (11)

The use of a Dammann grating sets a resolution limit on the input image. The maximum transitive spatial frequency in object plane is half of v_d. Increasing v_d may improve the object resolution, but it also yields a larger spectrum size D as indicated by Eq. (11). In practice, D has

16

a limit, therefore all the parameters such as M, N and v_d are limited to a certain range by the availability of usable space.

2.2 *Multi-channel pattern storage and recognition with VanderLugt correlator*

An architecture of a multi-channel VanderLugt-correlator-based two-stage HORAM system is shown in Fig.3, where F_1 and F_2 are the first and second spectrum planes respectively. An additional imaging arrangement from plane F_2 to plane H is used here for the convenience of placing the shutter array in plane F_2. We may record MN×MN different spectra in plane H by using two shutter arrays at planes F_1 and F_2, respectively, only a single aperture in each shutter array is open when each input image is applied. Assume the same reference beam is used in the recording process for all the input images and all the apertures of the shutters are opened simultaneously in the correlation step. Applying an arbitrary input O_{ij} among the memorized images, we will obtain one autocorrelation term and (M^2N^2-1) crosscorrelation terms in the center of plane P (i.e., the focus of the reference beam). The resultant correlation output is

$$u_c = O_{ij} \otimes O_{ij} + \sum_{\substack{m,n=1 \\ m,n,k,l \neq i,j,i,j}}^{MN} \sum_{k,l=1}^{MN} O_{mn} \otimes O_{kl}, \tag{12}$$

where $\otimes$ denotes correlation. Although the first term in the above equation is considerably larger than any other, the combination of the other terms will be larger than the first one due to the large number M^2N^2. Therefore this setup is not usable for large capacity pattern recognition. There are two remedying means to circumvent this problem.

First, we may open the shutter aperture sequentially for a given input pattern while observing the correlation output in plane P. The position of the opened aperture corresponding

to the maximum correlation reveals the specific input object. Evidently we must scan the whole shutter aperture array for each input image, and it takes a minimum time period of

$$T = M^2 N^2 \tau, \qquad\qquad (13)$$

where τ is the time required for the detection of the correlation peak. This time is dependent on some practical factors such as the recording material and the detecting device. If a CCD of a response time of 10 ms is used for correlation peak detection, T would be 10 seconds for $M^2 N^2 = 10^3$. This should be acceptable for some practical applications, but not fast enough for high-speed recognition and high data transfer operation.

An effective approach to solve this problem is to use the reference beam angular multiplexing technique. In this method we employ a different angle for each reference beam with each shutter aperture which is opened successively for each different input image in the recording process. The different reference beams form a focal array in plane P. In the correlation process all the shutter apertures are opened simultaneously for a given input, and the location of the brightest spot in P identifies the recognized input pattern. This technique can work much faster compared to the fixed reference beam method, but it is at the expense of using a complicated angle-adjusting recording system.

In the above analysis we have assumed that a planar hologram is used. In fact we may also use 3-D holographic recording materials such as the photorefractive crystals[13] for making the matched filters. The volume effects of a 3-D recording material enable us to realize angular multiplexing recording for each individual spectrum position. This property adds one more dimension to the storage capacity of the device, which may be estimated as follows.

For a Dammann grating with spatial frequency v_d, the minimum resolvable size in the object plane is $1/v_d$, and the information amount per binary input page is $(D_o v_d)^2$ bits, where D_o is the

18

dimension of input image (assume $D_{ox}=D_{oy}=D_o$). Since a 2-D recording plate can store $(MN)^2$ images, the storage capacity should be

$$C = (MN)^2 (D_o v_d)^2 \qquad (14)$$

bits, provided the lens aperture is large enough to transmit the spatial frequency v_d. On the other hand, for a 3-D device, there may be K×L holograms recorded by angular multiplexing for each spectrum position, where K and L are the angular changes in x and y directions respectively. Consequently the storage capacity is increased up to

$$C_v = (MN)^2 KL(D_o v_d)^2 \qquad (15)$$

bits. The values of K and L are mainly determined by the thickness of the crystal. Other limitations to MN and KL are the dimensions of the recording device and related optical elements.

For an example, assume $D_o=25$ mm, $v_d=15$/mm, M=9, N=5, then the storage capacity of this 2-D recording system is $C=2.8\times10^8$ bits. For making sufficient spectra separation in the 3-D recording with a crystal, we may reduce MN to, for instance, 4×4=16, and take a reasonable value of KL to be $10^2 \sim 10^3$, the resultant storage capacity C_v is $3.6\times10^9 \sim 10^{10}$ bits for a crystal of 1 cm^3. In comparison, the best result obtained recently by IBM using a single stage system with a photorefractive crystal[23] is 8.5×10^7 bits/cm^3. Hence, the multi-stage architecture can provide a new degree of freedom for improving the storage capacity.

2.3 *Multi-channel associate memory*

Conceptually an associate memory may be realized with the use of a nonlinear threshold element for feedback retrieval via a phase conjugate mirror (PCM). A viable architecture is shown in

Fig.4 where the multi-stage HORAM system is simplified as a spectrum replication system. A PCM is located in plane Pc and each filter in plane H is sequentially made for a different object and with a different reference angle. When a partial image corresponding to one of the stored images is applied to the input, a bright spot will appear at a proper position (the focus of its recording reference beam) in plane Pc. As a nonlinear and feedback device, the PCM reflects only this beam and suppresses all other beams. The reflected light will form a plane wave, conjugate to the original reference beam, and then generate a more complete image at the output plane via a beam splitter.

Although this concept is simple, the practical limitation seems to be the availability of a high-quality PCM with an effective aperture large enough to cover the whole correlation array.

2.4 Multi-channel joint transform hologram and image retrieval

The basic concept of making joint transform hologram (JTH) in a multi-channel system is illustrated in Fig.5 (a), where two input images are placed side by side in plane P_{in}. Their joint transform spectrum, which appears at the central region of the Fourier plane H, is recorded in a holographic medium.

With the use of a multi-stage HORAM system for spectrum replication, a multi-channel JTH can be made, where each element hologram in one position of the spectrum array corresponds to a specific pair of input images. As many as $(MN)^2$ image pairs can be recorded in a 2-D holographic medium. This multi-channel JTH may then be used for joint transform correlation (JTC) or image retrieval. For the purpose of JTC, we can use a plane wave to illuminate the JTH and obtain two correlation terms at the two opposite sides of the output plane located at the back focal plane of a Fourier transform lens behind the JTH. Since the location of the correlation spot

is only determined by the spatial separation between the two input images and independent of the element location in the JTH, the correlation outputs of all the JTH elements overlap if they are illuminated simultaneously. To avoid this effect, the JTH elements should be scanned successively (one by one) by using an electrical shutter array system.

The above scanning technique is also applicable for image retrieval. In this case we store $(MN)^2$ image pairs (a_i, b_j) (i,j=1 - MN) at different positions of the hologram H, and then input one image a_i and scan all the elements in the JTH. When the JTH element (i,j) is open, the reconstructed image b_j appears at the output plane as shown in Fig.5(b).

As we indicated above, although the successive scanning requirement may set a limit on the operation speed, the use of a high-speed detector will decrease the operation time and consequently increase the data processing speed.

3 Experimental demonstrations

3.1 *Geometrical parameters of the optical setup*

Our experimental setup of a two-stage HORAM system is shown in Fig.6, where G is a 9×9 Dammann grating with v_d =6.74/mm, and L_h is a 5×5 foci off-axis hololens. An off-axis hololens can be modeled by a combination of a prism for beam deflection, a conventional lens for beam focusing, and a 2-D orthogonal phase grating for focus multiplexing. As verified by our experiments, the equivalent grating spatial frequency of this hololens and its focal length for λ=514.5nm are v_h =19.7/mm and f_h =32.1cm respectively. Using M=9 and f_2=20cm in our case, we determined d_f ≥61.6cm from Eq.(10) for spectrum separation. In practice no serious overlap was seen in the range of d_f ≥60cm. An example photograph showing the well-separated 45×45=2025 spatial spectra obtained in plane H is given in Fig.7. The experimental parameters

we measured under exact matching condition are d_f=61.5cm, d_h=69.5 cm, D_f = 6.3 mm, and D=36.6 mm. From these parameters we have $(1/d_f + 1/d_h)^{-1}$ =32.6cm, and the Eqs. (1) and (11) give D_f=6.24mm and D=35.3mm. These results have shown a good agreement between our theoretical predictions and experimental measurements.

3.2 *Multi-channel pattern storage and recognition*

To verify the feasibility of the two-stage HORAM system for pattern storage and recognition, the optical setup shown in Fig.6 was used to make the multi-channel VanderLugt filters. The light source is an Ar^+ laser delivering about 0.8w power at 514.5nm. The test images are two letters, S and C, as shown in Fig.8. A plane wave is incident normally upon the combination of the object transparency and the Dammann grating. At plane F a square aperture is used to let only the central 9×9 array to pass through. After multiple imaging via the 5×5 foci hololens, we get the second spectrum array in plane H with 2025 individual and spatially-separated spectra. A plane reference beam is introduced to record the filters. The recording position in plane H may be chosen by using two circular apertures in planes F and H to pass only the selected spectrum order. First we select the (0,0) order in plane F and (-1,-1) order in plane H, the recording medium used is a Kodak 649F plate. Two filters were made with input letter S and C (one letter for each) respectively, and the exposure time is about 1/5 second. The correlation results with these two filters are shown in Figs. 9 and 10. Figure 9 corresponds to filter #1 made with letter S, where the left and right are autocorrelation for input S and crosscorrelation for input C, respectively. Obviously the former is much stronger than the latter, and their intensity ratio is about 6 to 1. Figure 10 shows similar results for filter #2 made with letter C, the autocorrelation is about 8 times stronger than the crosscorrelation.

To test the recognition capability of any non-central spectrum order, we next selected the (3,1) order in plane F and (1,-1) order in plane H to record filters #3 and #4 for the input images S and C successively. The Russian made FPR holographic plates were used with an exposure time of approximately 1.5 seconds. The corresponding correlation results are shown in Figs.11 and 12 for the two filters respectively. We can still clearly see that the intensity of autocorrelation is much higher than that of the crosscorrelation in each case. So if a proper threshold intensity is chosen, the input pattern can be recognized without any difficulty, and all the 2025 channels can work well.

3.3 Image retrieval with multi-channel VanderLugt filters and JTHs

In order to test the image retrieval capability of the two-stage multi-channel VanderLugt filters, we used a plane wave to illuminate the four filters we recorded one by one. The reconstruction results are shown in Fig.13 for filters #1 and #2 and in Fig.14 for filter #3 and #4, respectively. In each case we can clearly recognize the retrieved image, letter S or C. The reconstructed images in Fig.14 have lower signal-to-noise ratio than those in Fig.13, because filters #3 and #4 are made with off-axis spectrum orders in both planes F and H. These orders are weaker than those chosen from the central order in plane F and off-axis order in plane H.

We have also made some JTHs at different spectrum orders to verify the retrieval feasibility. Due to the low diffraction efficiency in our experiment (only amplitude holograms were used) and interference of the strong direct image with reconstructed pattern, the retrieved images with a two-stage HORAM system are very noisy, weak, and difficult to record. In the following we only present experimental results obtained with the JTHs recorded in the first spectrum plane F (the 9×9 array).

The first JTH was made in the architecture of Fig.5 with the letters C and E, shown in Fig.15 as the input image pair. The spectrum order was arbitrarily chosen as (-4,3). In the reconstruction step, if the input is letter C, we simultaneously obtain as shown in Fig.16 (a) a strong addressing image of letter C and a weak retrieved image of letter E at the output plane. When the letter E is used as the input, the output is shown in Fig.16 (b) where a strong E and a weak reconstructed C can be seen side by side.

Further we made the second JTH with input image pair of letters S and E as shown in Fig.17. In this recording process we did not block any spectrum in plane F so that all the 9×9 JTH elements were recorded at the same time. In the reconstruction step we have obtained the retrieved image by using any one JTH element. As examples, we present the experimental results obtained with the JTH of order (4,-2) in Fig.18 and the JTH of order (-3,-3) in Fig.19. In each photo we can clearly see the reconstructed image besides the strong direct image, regardless of which one of the image pair is used as the input. These results have shown that all the individual channels can work effectively and independently.

4 Conclusion

Based on the multi-stage HORAM system reported by Liu et al[21] , we have made more theoretical and practical analysis on the requirements of its geometrical parameters and its optical architecture constituents, its applications in multi-channel pattern recognition and associate memory, the 2-D and 3-D information storage capacity, and the multi-channel image storage and retrieval via VLC filters and joint transform holograms. A series of experiments have been performed to demonstrate the feasibility of the multi-channel pattern recognition and image retrieval with both of the VLC and JTC architectures. The experimental results with as many as 2025 channels have shown good agreement with the theoretical analysis. We have discussed the

potential applications of the system for large-capacity pattern storage, recognition, and retrieval.

The use of fast-response and low-noise recording materials and detecting devices will greatly improve the performance of the system for practical applications.

Acknowledgments

References

1. A. VanderLugt, "Signal detection by complex spatial filtering," IEEE Trans. Inf.Therory, **IT-10**, 139-145 (1964).

2. D. Casasent and D. Psaltis, "Position, rotation and scale invariant optical correlation," Appl.Opt. **15**, 1795-1799 (1976).

3. J. L. Horner and P. D. Gianino, "Phase-only matched filtering," Appl.Opt. **23**, 812-816 (1984).

4. L. Cai, Y. Jin, S. Zhou, P. Yeh, N. Marzwell, and H. K. Liu, "Translation sensitivity adjustable compact optical correlator and its application for fingerprint recognition," Opt.Eng. **35**, 415-422 (1966).

5. C. S. Weaver and J. W. Goodman, "A technique for optically convolving two functions," Appl.Opt. **5**, 1248-1248 (1966).

6. F. T. S. Yu and X. J. Lu, "A real-time programmable joint transform correlator," Opt.Commun. **52**, 10-16 (1984).

7. B. Javidi and C. J. Kuo, "Joint transform image correlation using a binary spatial light modulator at the Fourier plane," Appl.Opt. **27**, 663-665 (1988).

8. L. Z. Cai, Y. R. Wang, and H. Wang, "High efficiency hybrid joint transform correlator with preprocessed input image and replicated binary spectrum array," J.Modem Optics, **44**, 1197-1204 (1997).

9. D. Casasent, "Unified synthetic discriminant function computational formulation," Appl.Opt. **23**, 1620-1627 (1984).

26

10. B. V. K. V. Kumar, "Tutorial survey of composite filter design for optical correlators, " Appl.Opt. **31**, 4773-4801 (1992).

11. N. V. Kukhtarev, V. B. Markov, S. G. Odulov, M. S. Soskin, and V. L. Vinetskii, "Holographic storage in electrooptic crystals, I. Steady state," Ferroelectrics **22**, 949-964 (1979).

12. J. F. Heanue, M. C. Bashaw, and L. Hesselink, "Volume holographic storage and retrieval of digital data," Science **265**(5173), 749-752 (1994).

13. F. H. Mok, "Angle-multiplexed storage of 5000 hologram in lithium niobate," Opt.Lett. **18**, 915-917 (1993).

14. S. Yin, H. Zhou, M. Wen, Z. Yang, and F. T. S. Tu, "Wave-length multiplexed holographic storage in a sensitive photorefractive crystal using a visible light tunable diode laser," Opt.Comm. **101**, 317-321 (1993).

15. P. A. Mitkas and L. J. Irakliotis, "Three-dimensional optical storage for database processing," J. Opt. Memories Neural Net. **3**, 87-98 (1994).

16. J. H. Hong. I. McMichael, T. Y. Chang, W. Christian, and E. G. Paek, "Volume holographic memory system: Techniques and architectures," Opt. Eng. **34**, 2193-2203 (1995).

17. J. R. Wullert II and Y. Lu, "Limits of capacity and density of holographic storage," Appl. Opt. **33**, 2192-2196 (1994).

18. F. T. S. Yu and S. Yin, "Thick Volume photorefractive crystal wave-length-multiplexed reflection-type matched filter," Optical Memory Neural Networks **3**, 207-214 (1994).

19. L. Z. Cai, Y. R. Wang, and H. K. Liu, "Moving target recognition and tracking with photorefractive joint transform correlator," Proc.SPIE, **2896**, 189-196 (1996).

20. A. Pu, K. Curtis, and D. Psaltis, "Exposure schedule for multiplexing holograms in photopolymer films," Opt.Eng. **35**, 2824-2829 (1996).

21. H. K. Liu, Y. H. Jin, and N. I. Marzwell, "Advanced ultra-high-capacity optical random access memory and pattern recognition techniques," Opt.Eng. **37**, 779-788 (1998).

22. D. Gregory, G. Duthie, and H. K. Liu, "Large memory real-time multichannel multiplexed pattern recognition," Appl.Opt. **23**, 4560-4570 (1984).

23. IBM Holographic Optical Team, "Holographic storage promises high data density," Laser Focus World, **32**. 81-93 (1996).

Figure Captions:

Fig.1 Schematic diagram of a two-stage HORAM system. (a) Optical architecture; (b) spectrum distribution in plane F; (c) spectrum distribution in plane H.

Fig.2 Two configurations for adjusting the magnification between planes F and H.

Fig.3 The optical architecture of a two-stage HORAM system.

Fig.4 An optical multi-channel associate memory system using a PCM for image retrieval.

Fig.5 Multi-channel joint transform hologram: (a) Recording process; (b) reconstruction process.

Fig.6 Experimental setup for a two-stage multi-channel HORAM system.

Fig.7 An example photograph showing 2025 well-separated spatial spectra obtained by two-stage spectrum multiplexing.

Fig.8 Input images for VanderLugt matched filter fabrication.

Fig.9 Two-stage correlation results obtained from a VanderLugt filter #1 made with reference image "S" as shown in Fig.8, where the spectrum orders (0,0) and (-1,-1) are selected at plane F and H respectively. (a) Autocorrelation for input "S"; (b) crosscorrelation for input "C".

Fig.10 Two-stage correlation results obtained from a VanderLugt filter #2 made with reference image "C" as shown in Fig.8, where the spectrum orders (0,0) and (-1,-1) are selected at plane F and H respectively. (a) Autocorrelation for input "C"; (b) crosscorrelation for input "S".

Fig.11 Two-stage correlation results obtained from a VanderLugt filter #3 made with reference image "S" as shown in Fig.8, where the spectrum orders (3,1) and (1,-1) are selected at plane F and H respectively. (a) Autocorrelation for input "S"; (b) crosscorrelation for input "C".

Fig.12 Two-stage correlation results obtained from a VanderLugt filter #4 made with reference image "C" as shown in Fig.8, where the spectrum orders (3,1) and (1,-1) are selected at plane F and H respectively. (a) Autocorrelation for input "C"; (b) crosscorrelation for input "S".
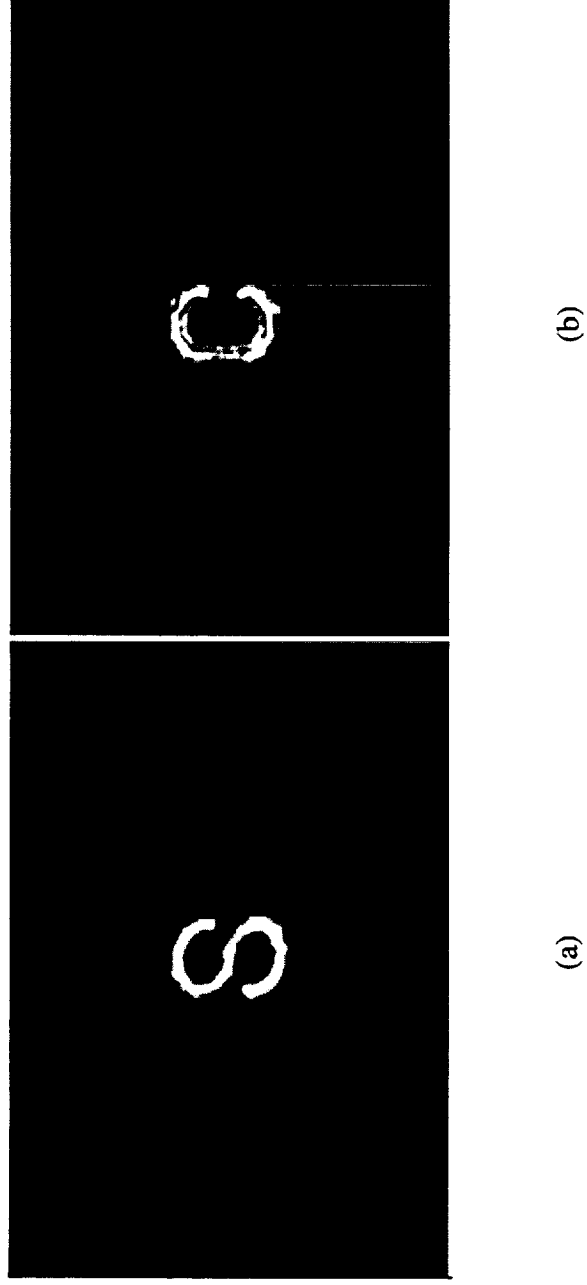
Fig.13 Reconstructed images with a plane reference wave input to (a) filter #1 and (b) filter #2.
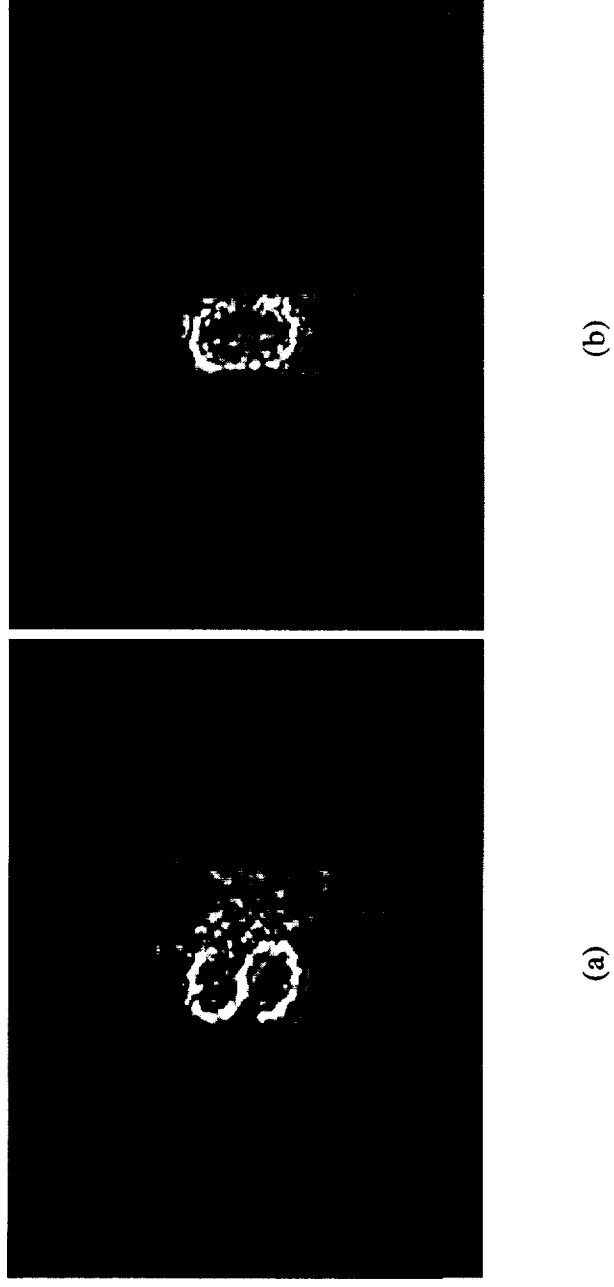
Fig.14 Reconstructed images with a plane reference wave input to (a) filter #3 and (b) filter #4.

Fig.15 Input image pair for the fabrication of joint transform hologram #1.
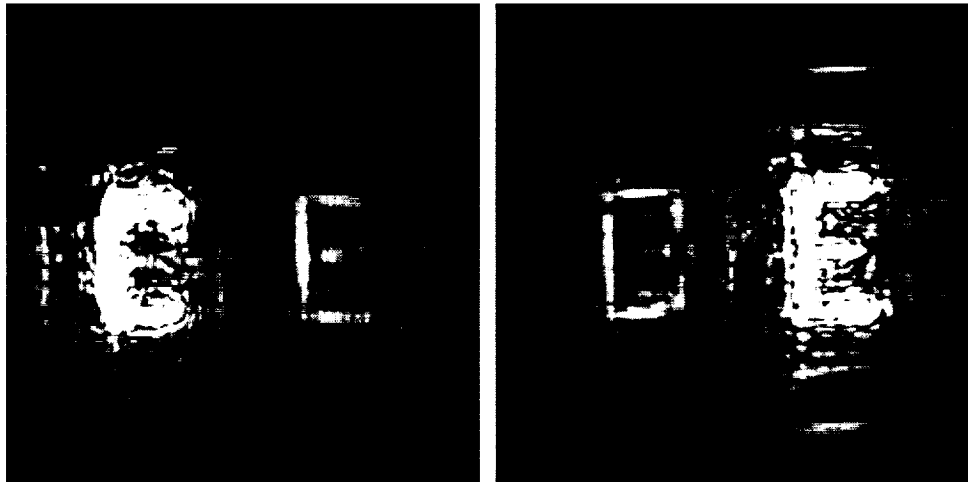
Fig.16 Reconstruction results obtained from the joint transform hologram #1 by using the spectrum order (-4,3): (a) With input "C"; (b) with input "E".

Fig.17 Input image pair for the fabrication of joint transform hologram #2.
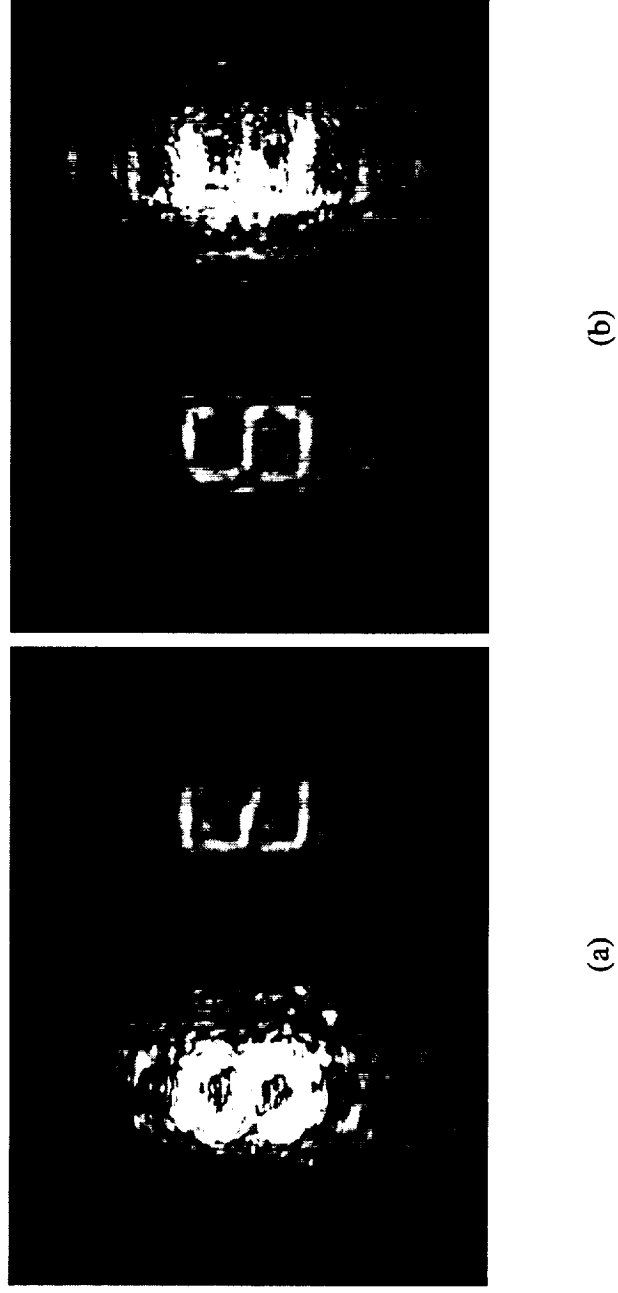
Fig.18 Reconstruction results obtained from the joint transform hologram #2 by using the spectrum order (4,-2): (a) With input "S"; (b) with input "E".

Fig.19 Reconstruction results obtained from the joint transform hologram #2 by using the spectrum order (-3,-3): (a) With input "S"; (b) with input "E".
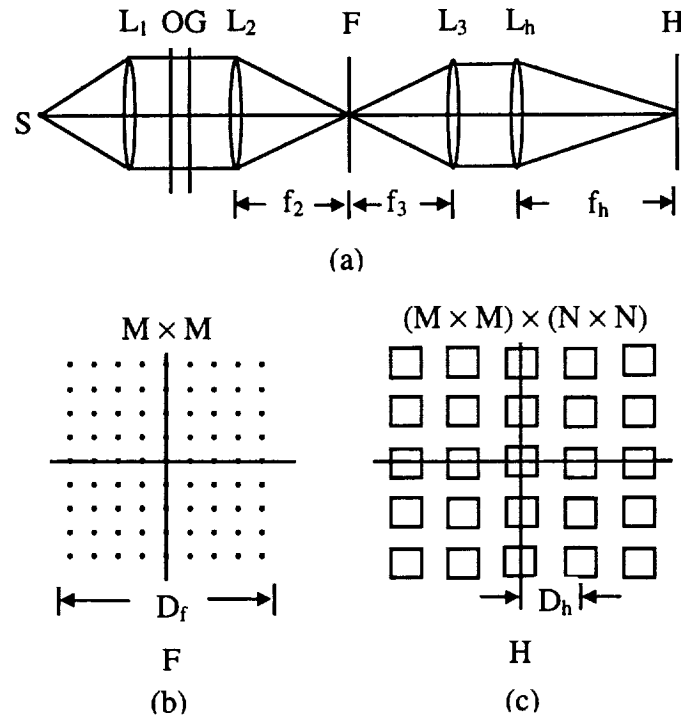
Fig. 1 Schmetic disgram of two-stage HORAM system. (a) Optical architecture;
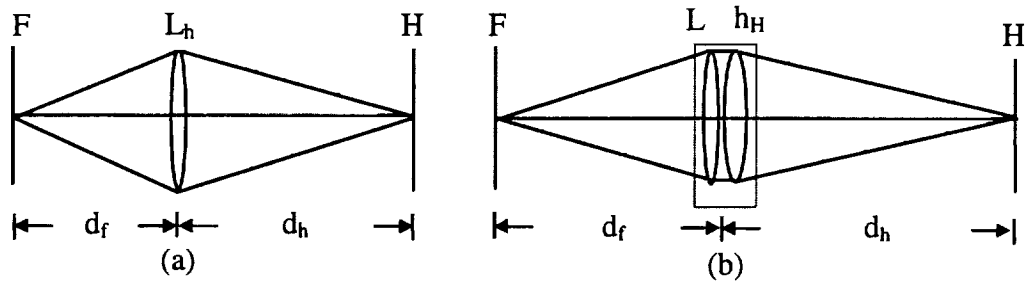(b) spectrum distribution in plane F; (c) spectrum distribution in plane H.

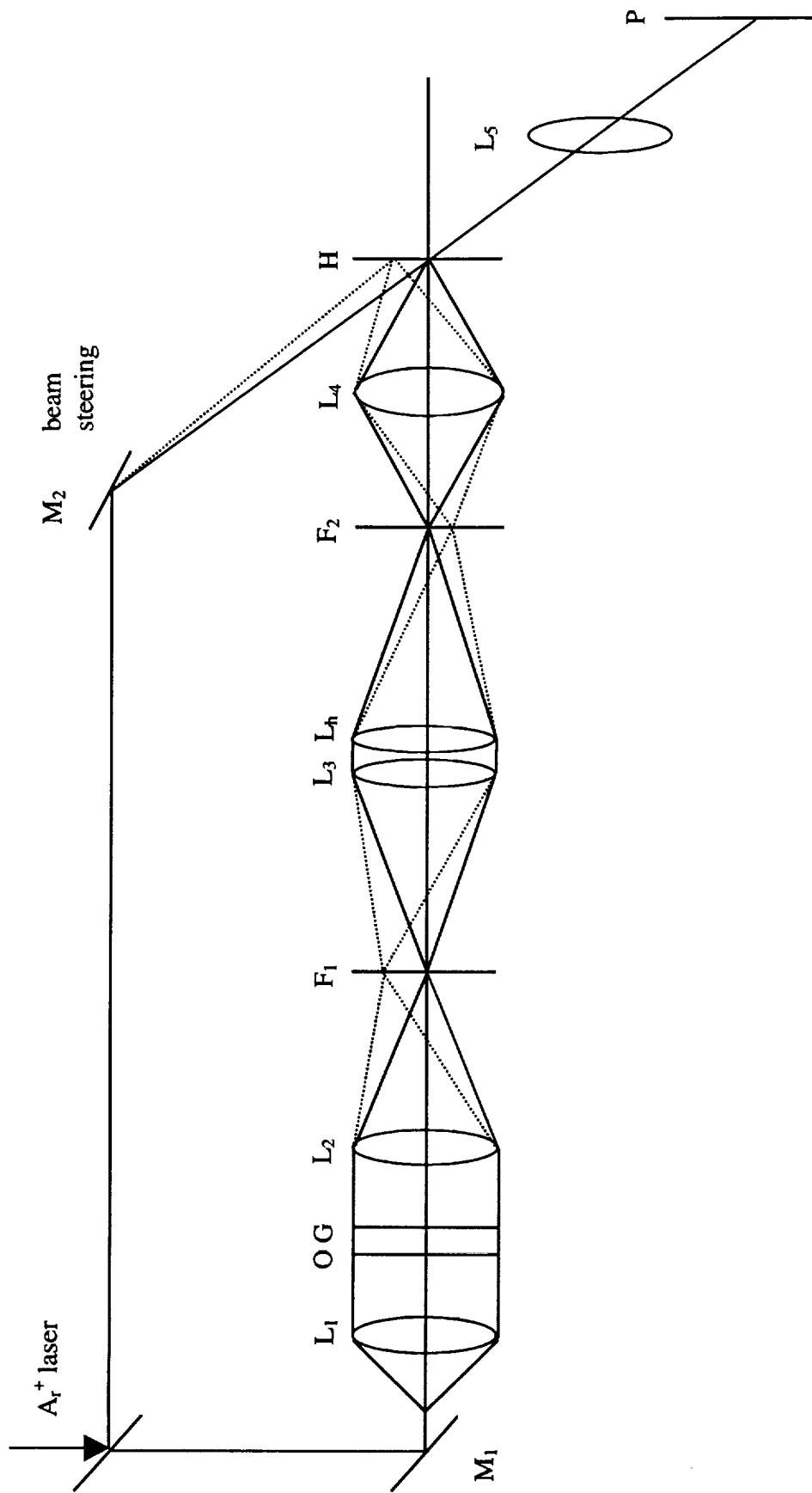Fig. 2 Two configurations for adjusting the magnification between planes F and H.

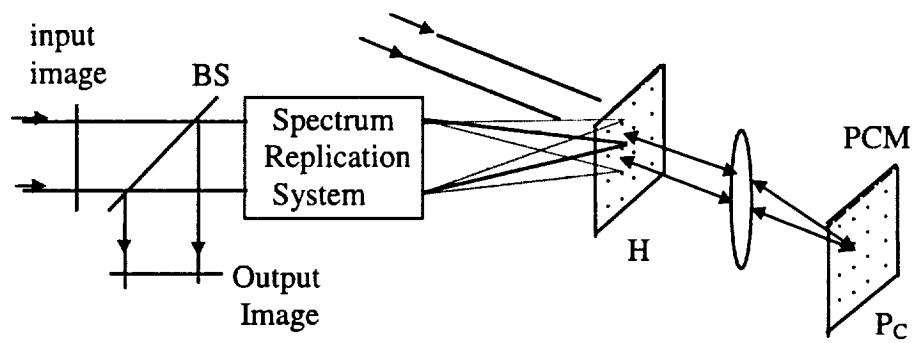Fig. 3 The optical architecture of a two-stage HORAM system.

33

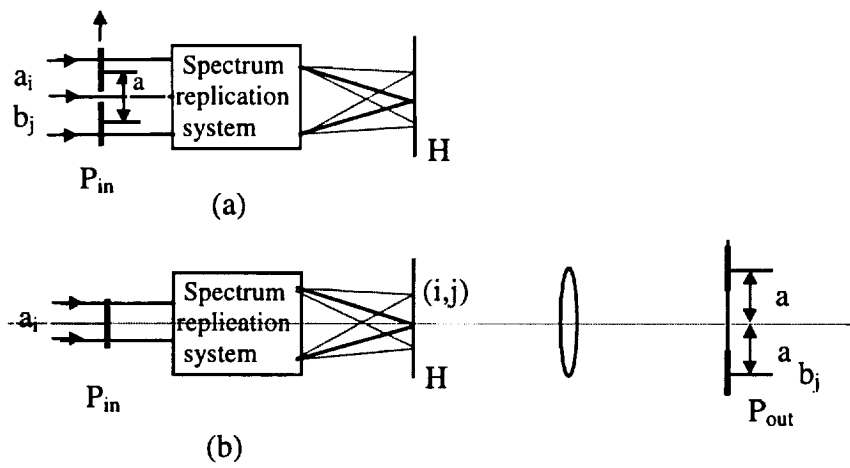Fig.4　An optical multi-channel associate memory system using a PCM for image retrieval.

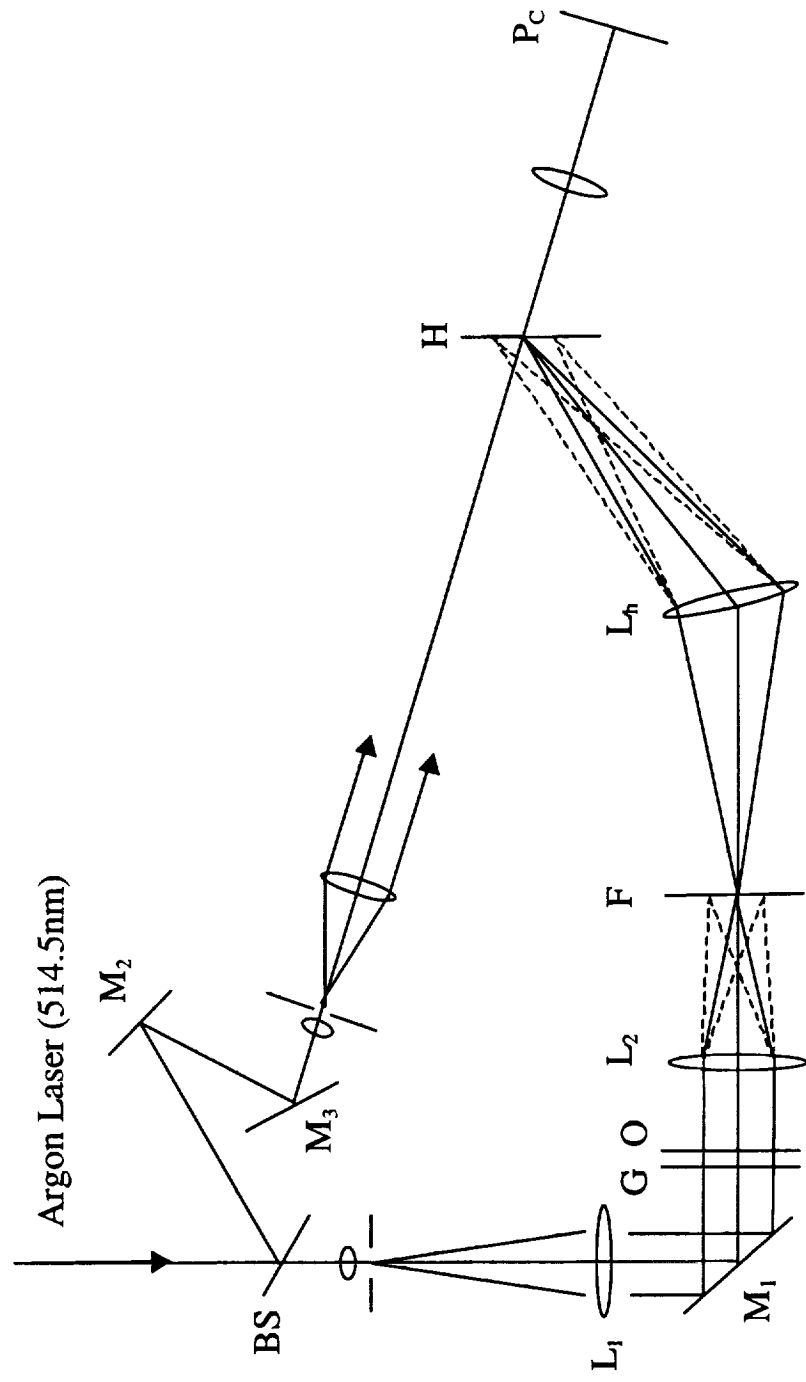Fig. 5 Multi-channel joint transform hologram: (a) Reading process; (b) reconstruction process.

Argon Laser (514.5nm)

M_2

M_3

BS

L_1

G O

F

M_1

L_2

L_h

H

P_c

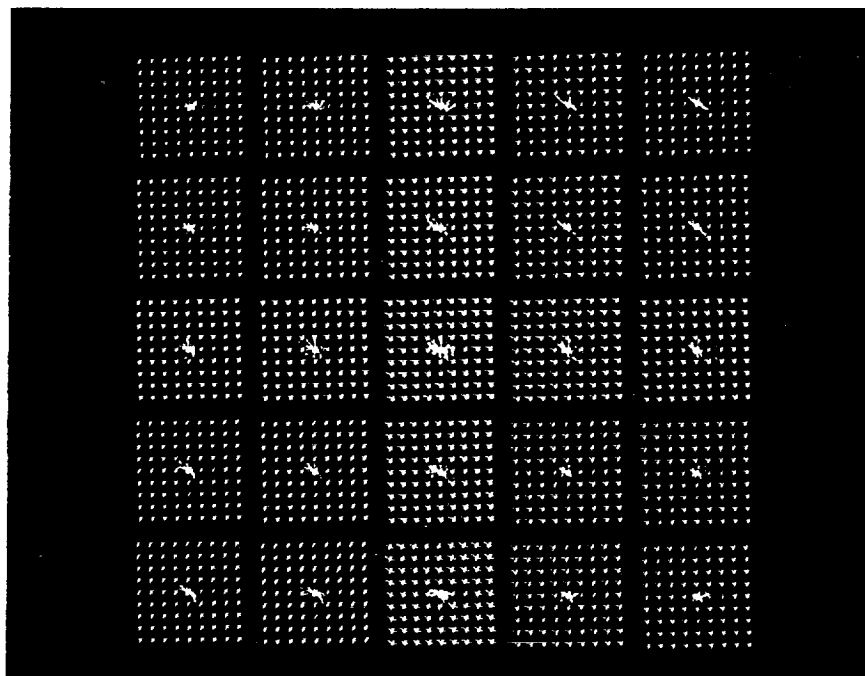Fig. 6 Experimental setup for a two-stage multi-channel HORAM system.

36

Fig. 7 An example photograph showing 2025 well-separated spectra obtained by two-stage spectrum multiplexing.

Fig.8　Input images for VanderLugt matched filter fabrication

(a)   (b)

Fig.9   Two-stage correlation results obtained from a VanderLugt filter #1 made with reference images "S" as shown in Fig. 8, where the spectrum orders (0,0) and (-1,-1) are selected at plane F and H respectively. (a) Autocorrelation for input "S"; (b) crosscorrelation for input "C".

39

(a)   (b)

Fig.10 Two-stage correlation results obtained from VanderLugt filter #2 made with reference image "C" as shown in Fig. 8, where the spectrum orders (0,0) are selected at plane F and H respectively. (a) Autocorrelation for input "C"; (b) crosscorrelation for input "S".
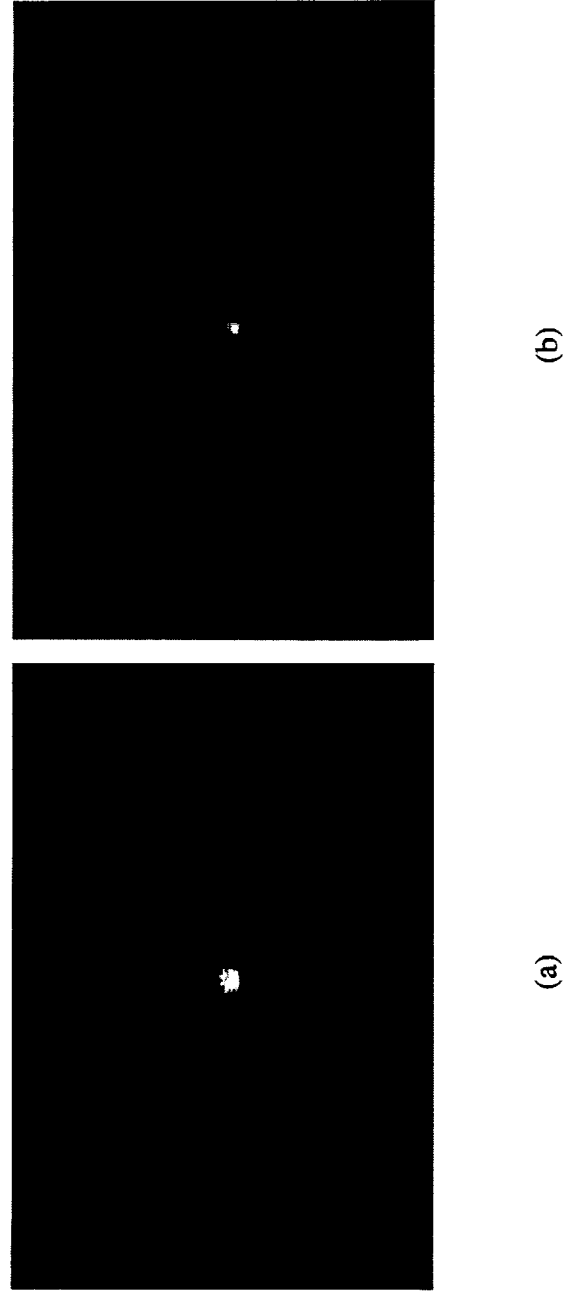
40

(a)   (b)

Fig.11   Two-stage correlation results obtained from a VanderLugt filter #3 made with reference image "S" as shown in Fig. 8, where the spectrum orders (3,1) and (1,-1) are selected at plane F and H respectively. (a) Autocorreltaion for input "S"; (b) crosscorrelation for input "C".
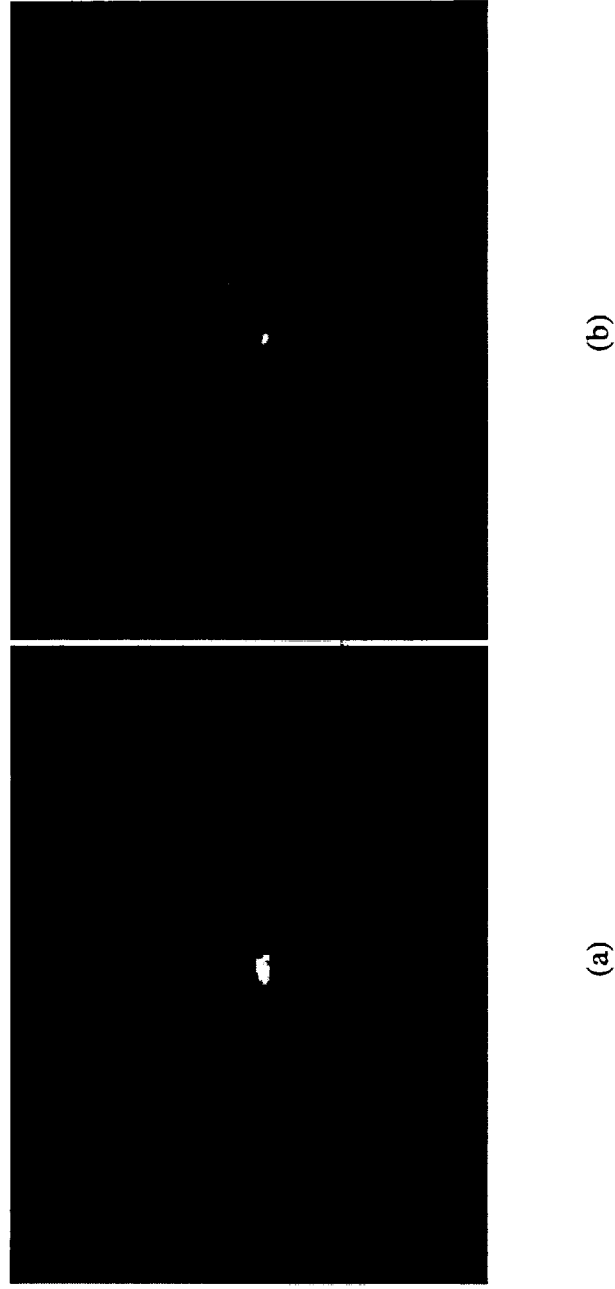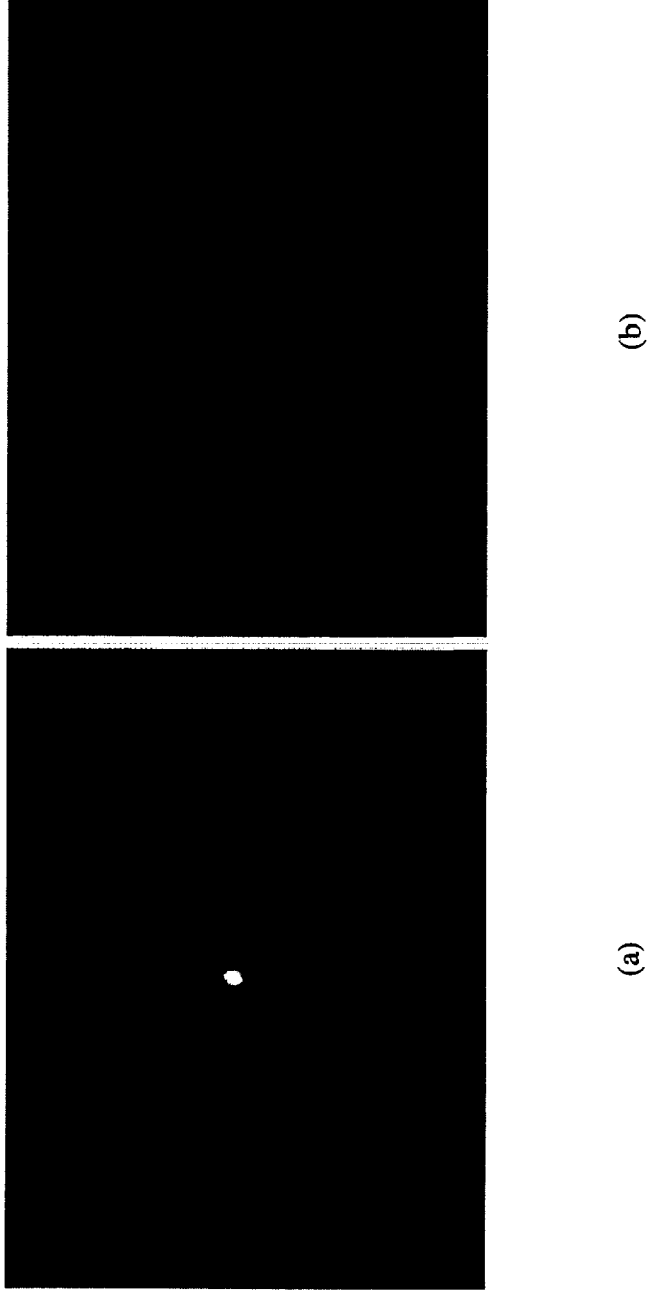
41

(a)

(b)

Fig.12 Two-stage correlation results obtained from a VanderLugt filter #4 made with reference image "C" as shown in Fig. 8, where the spectrum orders (3,1) and (1,-1) are selected at plane F and H respectively. (a) Autocorrelation for input "C"; (b) crosscorrelation for input "S".

42

(a)

(b)

Fig.13 Reconstructed images with a plane reference wave input to (a) filter #1 and (b) filter #2.

43

(a)

(b)

Fig.14 Reconstructed images with a plane reference wave input to (a) filter #3 and (b) filter #4.

44

Fig.15 Input image pair for the fabrication of joint transform hologram #1.

<div align="center">(a)   (b)</div>

Fig.16 Reconstruction results obtained from the joint transform hologram #1 by using the spectrum order (-4,3): (a) With input "C"; (b) with input "E".

Fig.17 Input images pair for the fabrication of joint transform hologram #2.

(a)

(b)

Fig.18 Reconstruction results obtained from the joint transform hologram #2 by using the spectrum order (4,-2): (a) With input "S"; (b) with input "E".

48

(a)

(b)

Fig.19 Reconstruction results obtained from the joint transform hologram #2 by using the spectrum order (-3,-3): (a) With input "S"; (b) with input "E".

49

5 TRANSLATION SENSITIVE ADJUSTABLE COMPACT OPTICAL CORRELATOR

The present invention is directed to pattern
recognition apparatus, and more particularly to opto-
electronic correlators for recognition of partially obscured
or modified objects.

10   Background and Summary of the Invention

An optical correlator compares an optical pattern to
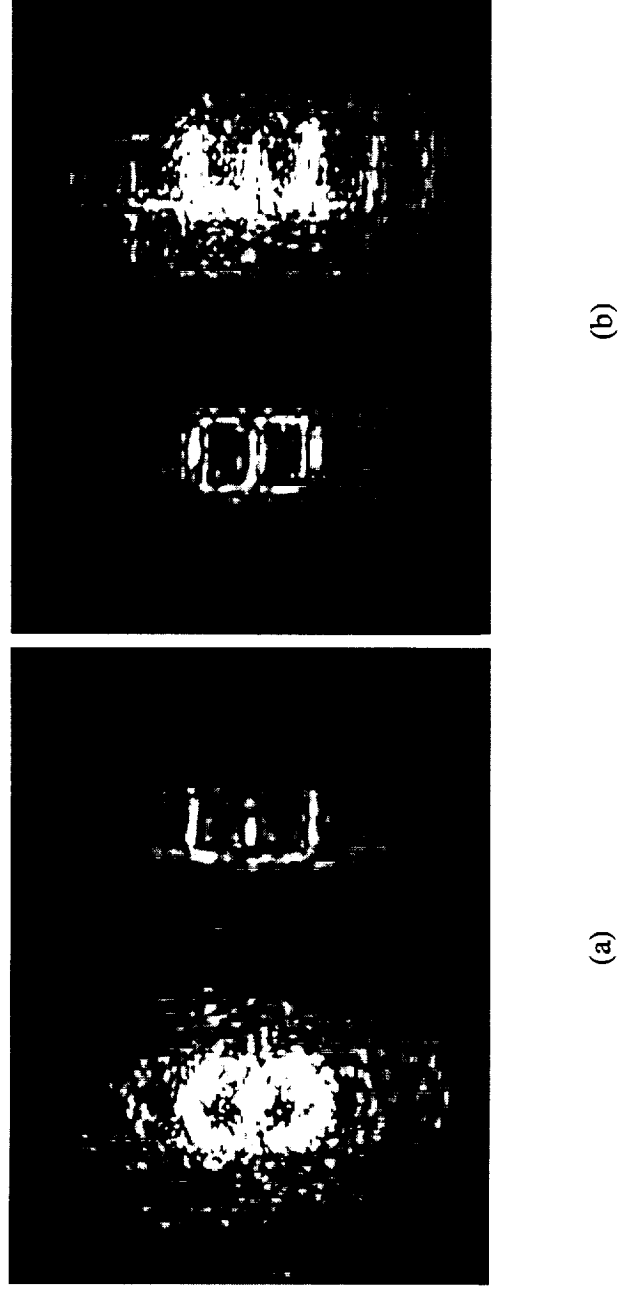a stored pattern to determine an amount of matching.
Optical correlators are essentially fast computers -- they
allow very fast identification of optical elements relative
15 to a stored sequence ("kernel").

Correlators operate in record and reconstruction
modes. During the record mode, an input image is recorded
in an optical element. The reconstruction mode matches
input information against the kernel to thereby determine
20 matches between the input information and the kernel.

Generally, optical correlators of the prior art have
used a plane wave to record an image in the matched spatial
filter and a lens behind the matched spatial filter to
collect data associated with the matching function performed
25 by the filter. These optical systems, however, have been
relatively sensitive to variations in the positioning of the
spatial filter and the input image. Lateral and
longitudinal variations in the positioning of the spatial
filter and the input image degrade the recognition
30 performance of the correlators.

Previous uses of prior art correlators have been
substantially limited by these accuracy requirements, and
other difficulties of implementation, such as size.

50

However, many applications seem well-suited to
analysis using such a system. For example, pattern
recognition, such as fingerprint recognition or robotic
vision applications are well suited to this operation,
5   because of the quasi periodic nature of these patterns.
This quasi periodic nature has suggested to the inventors
that frequency domain analyzers, such as correlators, would
be advantageous.

Unfortunately, the fingerprint recognition
10   environment is characterized by such variations as noted
above, due to variables in positioning and repositioning of
the finger in the imaging plane.

In addition, often in applications of imaging
technology the image seeking to be identified may be
15   partially obscured or unreadable. For example, in a
fingerprint recognition system, the image seeking to be
verified may be misaligned or offset relative to the imaging
plane. The image may also be obscured due to a cut or
abrasion on the surface of the skin. Accordingly, partial
20   images or partially obscured images may be presented for
verification. Control devices such as mechanical stops
(finger box) and the like can be used to minimize alignment
problems, but their effectiveness is limited. For
fingerprint recognition systems it would be desirable to
25   obtain matches for partially obscured images if a sufficient
portion of the image is readable.

In view of the above, the inventors recognized that
it would be desirable to provide a portable and compact
imaging system for use in robotic vision or fingerprint
30   recognition systems. Such an imaging system would have
adjustable sensitivity to variations in the displacement of
the filter or image and be capable of resolving partially
obscured images.

- 2 -

The present invention describes a sensitivity adjustable compact opto-electronic correlator and pattern recognition system for identification of a partially obscured or modified objects and includes a laser source, a

5 spatial light modulator, a transform lens, a holographic matched filter, and a detector located at a classification output plane. The laser source outputs a laser beam which is split by a beam splitter into an imaging optical path and a reference optical path during a recording process. The

10 imaging optical path uses a laser beam output from the laser source which is collimated through a collimating lens to provide a collimated laser beam which passes through a spatial light modulator for enhancing the beam and also entering an input image that is to be identified. The

15 collimated laser beam acts as a carrier for the input image which then passes through a transform lens having a focal length D1 at a first (holographic) plane. A complex structure associated with the input image is located within the cross-section of the focal point at the first plane.

20 The reference optical path includes a reference beam which is reflected through a second transform lens whose output is directed toward and interferes with the carrier beam at the first plane. The second transform lens is configured such that the reference beam is focused a predetermined distance

25 D2 beyond the first plane. In one aspect of the invention, a converging reference beam with adjustable focal length distance is used instead of a collimated reference beam as conventionally done in other existing correlators. The adjustable focal distance provides the desired sensitivity.

30 A film is placed at the holographic plane to record the interference pattern generated by the interference of the imaging optical path and the reference optical path. Thereafter, the film may be developed and acts as a

- 3 -

holographic matched filter when replaced back at the
holographic plane for use in recognizing an associated
object or image.

More specifically, a laser source which is used in
5   the recognition process provides a laser beam which is
collimated through a collimating lens and input into a
spatial light modulator. The spatial light modulator
receives as an input an image for verification, such as a
fingerprint, and utilizes the collimated laser beam as a
10   carrier to carry the image to a lens which focuses the image
to a focal point in the holographic plane.

An electronic shutter associated with the
holographic plane thereafter exposes an associated portion
of the film located at the holographic plane. The carrier
15   beam which contains the complex structure associated with
the image to be verified. Upon detecting a match, an output
is driven to a classification output plane which includes a
photodetector array. The detector array detects a matching
configuration based on light energy refracted from the
20   holographic plane. In operation, the holographic matched
filter (exposed film) screens improper images and provides
minimal output to the detector array unless a match
condition occurs.

In another aspect of the present invention a method
25   of recording images and for reconstructing the recorded
images includes recording a holographic image of an object,
and thereafter utilizing the holographic image in filtering
image data to verify matches with previously recorded image
data.

Brief Description of the Drawing

These and other aspects of the present invention will now be described in detail with reference to the accompanying drawings, in which:

5   FIG. 1 is a block diagram of a correlator according to one embodiment of the present invention.

FIG. 2 is a block diagram of the optical paths associated with a record mode for a correlator according to one embodiment of the present invention.

10   FIG. 3 is a block diagram of the optical paths associated with a reconstruction mode for a correlator according to one embodiment of the present invention.

FIG. 4 is a diagram of the lateral displacement of an input image relative to the intensity of the correlation

15   peak for a correlator according to one embodiment of the present invention.

Description of the Preferred Embodiments

FIG. 1 shows a block diagram of a laser opto-electronic correlator 50 including a laser 100 for providing

20   a laser beam output to a spatial light modulator 102 and holographic filter 104. The laser beam input to spatial light modulator 102 acts as a carrier for an input image 106 which is provided as an input to the spatial light modulator 102. A carrier beam output 108, including the image

25   information associated with input image 106, forms an input to holographic filter 104. The image-carrying laser beam through spatial light modulator 102 is Fourier transformed spatially by Fourier lens 103 which is placed at a distance of one focal length in front of the holographic filter plane

30   104. Holographic filter 104 also receives a reference beam from laser source 100 as an input thereof. The reference beam passes through a lens 105 which is placed at an

adjustable distance in front of the holographic filter plane
104. The function of lens 105 is to focus the reference
beam at a point whose distance from the holographic filter
104 is adjustable. Holographic filter 104 matches input
5   image 106 with an image that was previously stored on
holographic filter 104. The sensitivity of the matching of
the input to the stored input becomes adjustable with the
adjustment of the position of lens 105 in the reference
beam. The storage of the holographic image on holographic
10   filter 104 will be described in greater detail below in
association with the recording process.

   When a match is detected, the holographic filter
plane provides an output signal to a detector 110 indicating
that a match has occurred between the input image data and a
15   previously-recorded holographic image.

   FIG. 2 shows a block diagram of correlator 50
according to one embodiment of the present invention. A
laser source 210 provides a laser beam output which is
directed towards a beam splitter 220. In one embodiment the
20   laser source is a miniature laser diode source; a helium
neon laser, or other lasers may also be used.

   Beam splitter 220 splits the laser beam into an
imaging beam 222 along imaging path 200 and a reference beam
224 along reference path 202. Imaging beam 222 is directed
25   towards a mirror 230 which reflects the imaging beam 222
towards spatial filter 235. Spatial filter 235 spreads the
imaging beam, generally directing the now-spread imaging
beam towards a collimating lens 240. Collimating lens 240
collects the imaging beam light energy and directs it
30   parallel to the perpendicular axis of the lens, providing a
collimating laser beam for input into a spatial light
modulator 245.

In one embodiment, spatial light modulator 245 is a
90° prism. The 90° prism is oriented such that the
collimated laser beam output from collimating lens 240 is
provided as an input onto a first side 246 of the prism.

5   The prism includes an imaging surface 247 for receiving an
image for recording or comparison operations. The imaging
surface 247 is on the long hypotenuse side of the prism
opposite the 90° angle.

The imaging data, e.g. a fingerprint is acquired on

10   imaging surface 247 which may include a finger box (not
shown) for maintaining the relative position of a finger
relative to the imaging surface.

A second side 248 of the prism adjacent to first
side 246 provides a carrier beam output 249, combining the

15   image data received at imaging surface 247 with the
collimated laser beam output from collimating lens 240
received at first side 246. The prism realizes the real-
time input of an image via the total internal reflection
mechanism of the prism device. Specifically, the collimated

20   laser beam input from the collimating lens 240 acts as a
carrier for the image data, thereby providing a carrier beam
output which is directed towards a transform lens 250.

As was described above, spatial light modulator 245
provides an output carrier beam 249 as an input to transform

25   lens 250 having a focal length of D1. Transform lens 250
may be a Fourier transform lens which provides a spatial
Fourier transform of the image data which is focused on a
matched spatial filter (MSF) plane, generally indicated at
260. A cross section of a focal point of the output from

30   transform lens 250 includes complex structures associated
with the input image provided as an input to spatial light
modulator 245.

Film 265 is placed at MSF plane 260 and is exposed
to the focused carrier beam via an electronically controlled
shutter (not shown) associated with the MSF plane. The
electronically controlled shutter controls the exposure of
5   film 265 to light from the imaging optical path.

Referring now to the reference path, beam splitter
220 provides a reference beam 224 which is directed toward a
mirrors 232 and 234 for reflection towards the MSF plane
260. Specifically, after reflection from mirror 234, the
10   reference beam passes through a spatial filter 236 which
spreads the output beam. The light energy is there after
collected by a second transform lens 238 which focuses the
reference beam toward a detector 270. In one embodiment,
the transform lens is a Fourier transform lens. The
15   reference beam is aligned such that the light energy
directed from the transform lens 238 passes through MSF
plane 260 prior to being focused at detector 270. In one
aspect of the present invention, the position of the
transform lens 238 is adjustable in its optical axis such
20   that the sensitivity of detection may be adjusted.

The Recording Process

In order to record an image for comparison at a
future time, an image recording process is invoked. The
image recording process consists of providing an image, such
25   as a fingerprint, at the imaging plane of spatial light
modulator 245. During the recording process, the laser
source 210 outputs a laser beam which is split by beam
splitter 220 into an imaging beam 222 and reference beam
224. In the imaging optical path, the imaging beam is
30   collimated through collimating lens 240 to provide a
collimated laser beam output to spatial light modulator
(prism) 245. Spatial light modulator 245 enhances the

- 8 -

imaging beam and also receives as an input the fingerprint
that is to be recorded at imaging plane 247.

The collimated laser beam output from collimating
lens 240 acts as a carrier for the fingerprint image
5   providing a carrier beam as an output from spatial light
modulator 245 for transfer to transform lens 245. The focal
point for transform lens 245 is at MSF plane 260.

At the same time, the laser source 210 provides a
reference beam in the reference optical path which is
10   reflected through a second transform lens 238 whose output
is directed toward and interferes with the carrier beam at
MSF plane 260. In one embodiment, the second transform lens
is identical to the first transform lens. Second transform
lens 238 may be a Fourier transform lens. The second
15   transform lens is configured to focus the reference beam a
predetermined distance D2 beyond the MSF plane. Film 265
placed at MSF plane 260 is exposed to the interference
pattern created by the complex structure associated with the
input image (fingerprint) in the carrier beam and the
20   reference beam by the electronic controlled shutter
associated with MSF plane 260. Thereafter the film is
developed and replaced at the MSF plane for use in the
reconstruction process.

Reconstruction/Recognition Process
25   FIG. 3 shows the reconstruction process. Laser
source 210 provides a laser beam which is directed through a
pinhole spatial filter 235 toward a collimating lens 240.
Alternatively, the same set-up as described in the recording
process may be used including a beam splitter. However, the
30   reference optical path is not utilized in the reconstruction
process. Collimating lens 240 provides a collimated laser
beam output for input into spatial light modulator 245. A

fingerprint seeking to be verified (recognized) is provided
as an input to imaging plane 247 of spatial light modulator
(prism) 245. Spatial light modulator 245 receives the input
image and utilizes the collimating laser beam as a carrier
5   to carry image data to the transform lens 250. Transform
lens 250 focuses the image data to a focal point in MSF
plane 260.

       The electronically controlled shutter associated
with MSF plane 260 is opened to expose the film to the
10   focused carrier beam. In the absence of the interfering
reference beam, the exposed and developed film acts as a
filter to the imaging optical path, performing a matching
function associated with a previously recorded image.
Specifically, film 265, upon being exposed to the complex
15   structure in the focal point of the carrier beam (after
being developed), defracts light toward detector 270 as if
the reference beam were present if the fingerprint data in
the carrier beam is the same as the previously recorded
fingerprint data. In the event a match occurs, detector 270
20   receives a light pattern which is indicative of a match
condition.

Relationship between Recognition Sensitivity and the Lateral and Longitudinal displacement of the Filter and Input Image

       Repeatability of matching capability in correlator
25   50 is a primary concern for commercial applications. In
order to assure repeatability, the MSF plane (film 265)
should be located exactly at the focal point of transform
lens 250 when replaced in the correlator after developing.
Longitudinal and lateral displacements of the MSF plane may
30   result in poor repeatability characteristics for other
existing devices. One aspect of the present invention
provides a solution for the enhancement of repeatability of

recognition. An analysis of the effects of longitudinal and lateral displacement of the filter (film 265) indicated that the effect of longitudinal displacement on repeatability was much less than that of lateral displacement. However,

5   either may skew results. The inventors prefer the following technique for replacing film 265 at the focal point for the transform lens 250 by examining a correlation peak.

During the recording process, the focal point (at MSF plane 260) associated with the transform lens 250 is

10 located thereby defining MSF plane 260. Film 265 is fixed at this location before recording. After removal and development of film 265, film 265 is replaced in approximately its original location. The original image is applied to the spatial light modulator or through the prism.

15 A correlation peak is detected associated with the maximum intensity of light received at detector 270 when moving film 265 only laterally. This is accomplished by a manual review or by an automated vision process. The film can be returned to roughly its original position moving the filter

20 continuously in a lateral direction while observing the correlation peak intensity received by the detector centered at the focal point of the reference beam. Film 265 is thereafter moved until the intensity reaches its maximum at the detector. After repeated experiments with the system

25 using the above-described approach, it has been found that the translation sensitivity is dependent on the ratio D_2/D_1 of the system configuration. This will be elaborated further below.

In addition, shifts in the fingerprint image either

30 laterally or longitudinally will effect the repeatability of the correlator system. Specifically, lateral and longitudinal shifts in the input image will result in shifts in the correlation peak. In order to minimize the

- 11 -

repositioning error for objects, various control mechanisms
may be utilized including a confining box.

      In making the correlator system compact, a small
area detector instead of a detector array may be utilized.
5 The small area detector includes a small pinhole as a
receiving aperture. The size of the pinhole is configured
to be large enough to detect the correlation peak while able
to tolerate a certain amount of input displacement. In
addition, the size of the pinhole should be small enough to
10 reject most of the background noise. In one embodiment, for
the identification of fingerprints (where the fundamental
spatial frequency of two line pairs per millimeter occurs),
the width of the correlation peak is approximately 0.5
millimeters for the case where the D2/D1 equals 1. In this
15 embodiment, the diameter of the pinhole is approximately 1
millimeter.

Adjustment of the Translation Sensitivity via the Adjustment of Geometric Parameters D_1 and D_2

      In an embodiment which utilizes a pinhole detector,
20 the movement of the correlation peak due to laterally
shifted input images must be compensated for. As indicated
above, the correlation peak will move laterally with a
laterally shifted input image. Accordingly, as the
correlation peak moves laterally (tracking the movement of
25 the input image), the amount of light received at the
detector is diminished. This diminishment of light at the
detector due to a shifted input image is generally referred
to as translation sensitivity.

      Translation sensitivity is a performance parameter
30 which relates to the ability of the correlator to detect a
match, given a displacement of the input image. Given the
movement of the correlation peak due to a shifted input

image, it would not be convenient to adjust the pinhole
position each time to match the input displacement.
However, analysis has shown that translation sensitivity for
the correlator system of the present invention is strongly

5   dependent on the geometric configuration of the system,
namely the relationship of the parameters D2 and D1.
Translation sensitivity can be reduced by decreasing the
ratio of D2 to D1, resulting in an increase in the overall
repeatability of the correlator. Accordingly, the ability

10   to adjust the translation sensitivity of the optical
correlator via the adjustment of the ratio between D2 and D1
results in improved image recognition capability of the
system.

          FIG. 4 shows a diagram of lateral displacement of

15   input image (such as a fingerprint) relative to the
intensity of the correlation peak. Ratios of D2 to D1 of
less than approximately 1 will yield decreased translation
sensitivity. In one embodiment, the ratio is 1 to 4, or .25
The smaller the D2 to D1 ratio, the more tolerant the system

20   is to lateral displacements

Compensation for Zero Spatial Frequency Term of Images

          Another problem effecting the final correlation
results is the zero spatial frequency (DC) term of the
carrier beam, whose relative value is greater than 0.5 in

25   the practical prism input case. The correlation between
D.C. terms of two different images may introduce a
significant background peak intensity. A simple approach to
eliminate this effect is to overexpose film 265 in the MSF
plane during the recording step, so that the DC portion of

30   the center of the spectrum becomes entirely dark and hence
has no diffraction function.

Detection of Partially Obscured Images

At the detector the relevant intensity of the light
detected from a match or a non-match condition can be
described as follows. Assuming that a perfect match
5   provides a relative intensity of 1.0, the system of the
present invention typically returns (detracts) approximately
0.35 or 35% of the light in a no-match condition. For the
case of no-input image (background test), approximately 18%
of the imaging light is defracted through the MSF filter
10 plane. Accordingly, the present invention may be utilized
to recognize partially obscured images by setting a
threshold for detection to be between the ideal relative
intensity of 1.0 and the no-match return level of
approximately 35%. In one embodiment, the match threshold
15 is set at approximately between 50% and 90%, with 60%
preferred. At these levels, partially obscured objects
which otherwise may not have been detectable by other
recognition systems may be identified.

Alternative Embodiments

20   In one embodiment, transform lens 238 and 250 may be
multi-channel lens. Electronic shutter associated with MSF
plane 260 is used to expose a plurality of locations on film
265. Multi-channel lens create a plurality of focal points
at MSF plane 260, each focal point including complex image
25 information associated with the image input at the spatial
light modulator. The electronic shutter is used to expose
film 265 to only one of the focal points, storing the
information at a predetermined position on film 265.
Accordingly, a plurality of image interference patterns may
30 be stored on the same film 265. During reconstruction,
electronic shutter sequences through the various stored
images to detect a match. Alternatively, the electronic

- 14 -

shutter may be opened completely exposing all of the stored interference patterns. A match is detected based on the defracted light received at the detector just as described above.

5   The present invention has been described in terms of one or more embodiments. The invention, however, is not limited to the embodiments depicted or described. Rather, the scope of the invention is defined by the claims which follow.

What is claimed is:

1   1. An apparatus for recording images comprising:
2   a laser source producing a laser beam;
3   a spatial light modulator receiving an image for
4   recording and said laser beam, said laser beam acting as a
5   carrier for said image, said spatial light modulator
6   outputting a carrier beam including image data;
7   a first transform lens receiving said carrier beam,
8   said first transform lens having a predetermined focal
9   length D1 focusing said carrier beam at a first plane;
10   an adjustable transform lens for receiving said
11   laser beam and outputting a focused reference beam directed
12   toward and interfering with said carrier beam at said first
13   plane, said focused reference beam having a focal point an
14   adjustable distance D2 beyond said first plane; and
15   a film located at said first plane for recording an
16   interference pattern between said focused reference beam and
17   said carrier beam.

1   2.   The apparatus of claim 1 wherein said transform lens
2   and said adjustable transform lens are multi channel lens,
3   and where said electronic shutter exposes said film to a
4   single channel of data at a time.

1   3.   The apparatus of claim 1 where a ratio of D2 to D1
2   is approximately 50 to 90 percent.

1   4.   The apparatus of claim 1 where a ratio of D2 to D1
2   is approximately 60 percent.

1   5.   The apparatus of claim 1 where said detector is a
2   detector array.

- 16 -

1　6.　　　The apparatus of claim 1 where said detector is a
2　pin hole detector.

1　7.　　　The apparatus of claim 1 where said spatial light
2　modulator is a 90° prism.

1　8.　　　The apparatus of claim 1 wherein said laser source
2　is a helium neon laser.

1　9. An apparatus for reconstructing images comprising:
2　　　　　　a laser source providing as an output a laser beam;
3　　　　　　a spatial light modulator receiving as an input an
4　image for processing and said laser beam, said laser beam
5　acting as a carrier for said image, said spatial light
6　modulator outputting a carrier beam including image data;
7　　　　　　a transform lens receiving said carrier beam, said
8　transform lens having a predetermined focal length focusing
9　said carrier beam at a first plane;
10　　　　　a film located at said first plane including a
11　recorded interference pattern associated with an image; and
12　　　　　a detector located a predetermined distance from
13　said first plane for receiving light refracted from said
14　film, such that light is refracted and focused at said
15　detector if said image matches said recorded interference
16　pattern.

1　10. An apparatus for recording images comprising:
2　　　　　　a laser source providing as an output a laser beam;
3　　　　　　a beam splitter receiving said laser beam and
4　splitting it into an imaging beam and a reference beam;
5　　　　　　a collimating lens for receiving said imaging beam
6　and providing as an output a collimated laser beam;

- 17 -

7   a spatial light modulator receiving as inputs an
8   image for recording and said collimated laser beam, said
9   collimated laser beam acting as a carrier for said image,
10 said spatial light modulator outputting a carrier beam
11 including image data;
12   a transform lens receiving said carrier beam, said
13 transform lens having a predetermined focal length D1
14 focusing said carrier beam at a first plane;
15   a shutter array between said transform lens and said
16 first plane, said shutter array including an open position,
17 a closed position and means for switching between the two;
18   an adjustable transform lens for receiving said
19 reference beam and outputting a focused reference beam
20 directed toward and interfering with said carrier beam at
21 said first plane, said focused reference beam having a focal
22 point an adjustable distance D2 beyond said first plane; and
23   a film located at said first plane and exposed when
24 said shutter array is in said open position for recording an
25 interference pattern between said focused reference beam and
26 said carrier beam.

1   11. An apparatus for reconstructing images comprising:
2   a laser source providing as an output a laser beam;
3   a beam splitter receiving said laser beam and
4   splitting it into a imaging beam and a reference beam;
5   a collimating lens for receiving said imaging beam
6   and providing as an output a collimated laser beam;
7   a spatial light modulator receiving as an input an
8   image for processing and said collimated laser beam, said
9   collimated laser beam acting as a carrier for said image,
10 said spatial light modulator outputting a carrier beam
11 including image data;

12   a transform lens receiving said carrier beam, said
13 transform lens having a predetermined focal length focusing
14 said carrier beam at a first plane;
15   a shutter array between said first transform lens
16 and said first plane, said shutter array including an open
17 position, a closed position and means for switching between
18 the two;
19   a film located at said first plane including a
20 recorded interference pattern associated with an image; and
21   a detector located at a predetermined distance from
22 said first plane for receiving light refracted from said
23 film when said shutter array is in said open position, such
24 that light is refracted and focused at said detector if said
25 image matches said recorded interference pattern.

1 12. A method for recording an image comprising the steps
2 of:
3   providing a laser beam;
4   splitting said laser beam into an imaging beam and a
5 reference beam;
6   superimposing an image on said laser beam resulting
7 in a carrier beam;
8   focusing said carrier beam by a transform lens at a
9 first plane;
10   focusing said reference beam by an adjustable
11 transform lens and outputting a focused reference beam
12 directed toward and interfering with said carrier beam at
13 said first plane, said focused reference beam having a focal
14 point an adjustable distance beyond said first plane; and
15   recording an interference pattern between said
16 focused reference beam and said carrier beam at said first
17 plane.

1   13.   A method of verifying an image comprising the steps
2   of:
3   providing a laser beam;
4   superimposing an image to be verified on said laser
5   beam resulting in a carrier beam;
6   focusing said carrier beam through a transform lens
7   at a first plane;
8   providing a recorded interference pattern associated
9   with at least one image at said first plane, said recorded
10   interference pattern refracting light from said at least one
11   image to a detecting plane; and
12   detecting a match between said image and said
13   recorded interference pattern based upon an amount of light
14   refracted through said recorded interference pattern located
15   at said first plane and received at said detecting plane.

1   14.   A method for recording and reconstructing an image
2   comprising the steps of:
3   providing a laser beam;
4   splitting said laser beam into an imaging beam and a
5   reference beam;
6   collimating said imaging beam resulting in a
7   collimated laser beam;
8   superimposing an image on said collimated laser beam
9   resulting in a carrier beam;
10   focusing said carrier beam by a transform lens at a
11   first plane;
12   focusing said reference beam by an adjustable
13   transform lens and outputting a focused reference beam
14   directed toward and interfering with said carrier beam at
15   said first plane, said focused reference beam having a focal
16   point an adjustable distance beyond said first plane;

- 20 -

```
17              recording an interference pattern between said
18  focused reference beam and said carrier beam at said first
19  plane; and
20              detecting a match between a previously stored
21  interference pattern and a subsequent image by detecting
22  light refracted and focused through said recorded
23  interference pattern at a detection plane a predetermined
24  distance from said first plane.
```

TRANSLATION SENSITIVE ADJUSTABLE COMPACT OPTICAL CORRELATOR

Abstract of the Disclosure

5   A sensitivity adjustable compact opto-electronic correlator and pattern recognition system for identification of a partially obscured or modified objects includes a laser source, a spatial light modulator, a transform lens, a holographic matched filter, and a detector located at a

10   classification output plane. The laser source outputs a laser beam in an imaging optical path and a reference optical path for use during a recording process. The imaging optical path directs the laser beam output through a spatial light modulator for entering an input image that is

15   to be identified. The laser beam acts as a carrier for the input image which then passes through a transform lens having a focal length D1 at a first (holographic) plane. A complex structure associated with the input image is located within the cross-section of the focal point at the first

20   plane. The reference optical path includes a reference beam which is reflected through an adjustable transform lens whose output is directed toward and interferes with the carrier beam at the first plane. The adjustable transform lens is configured such that the reference beam is focused

25   an adjustable distance D2 beyond the first plane. A film is placed at the holographic plane to record the interference pattern generated by the interference of the imaging optical path and the reference optical path. Thereafter, the film may be developed and acts as a holographic matched filter

30   when replaced back at the holographic plane for use in recognizing an associated object or image.
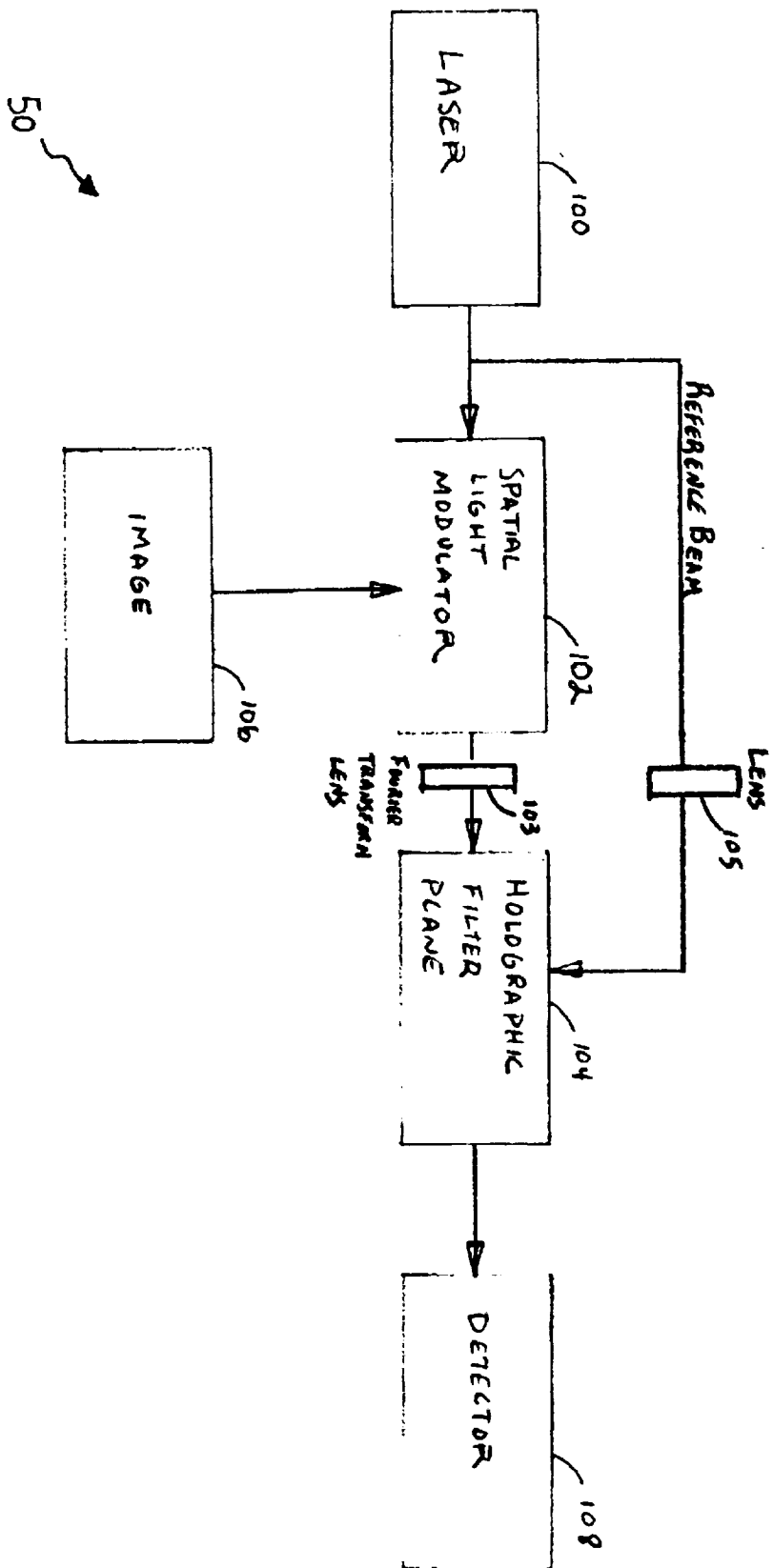
39225.P11

FIG. 1

50

LASER 100

SPATIAL LIGHT MODULATOR 102

IMAGE 106

REFERENCE BEAM

FOURIER TRANSFORM LENS 103

LENS 105

HOLOGRAPHIC FILTER PLANE 104
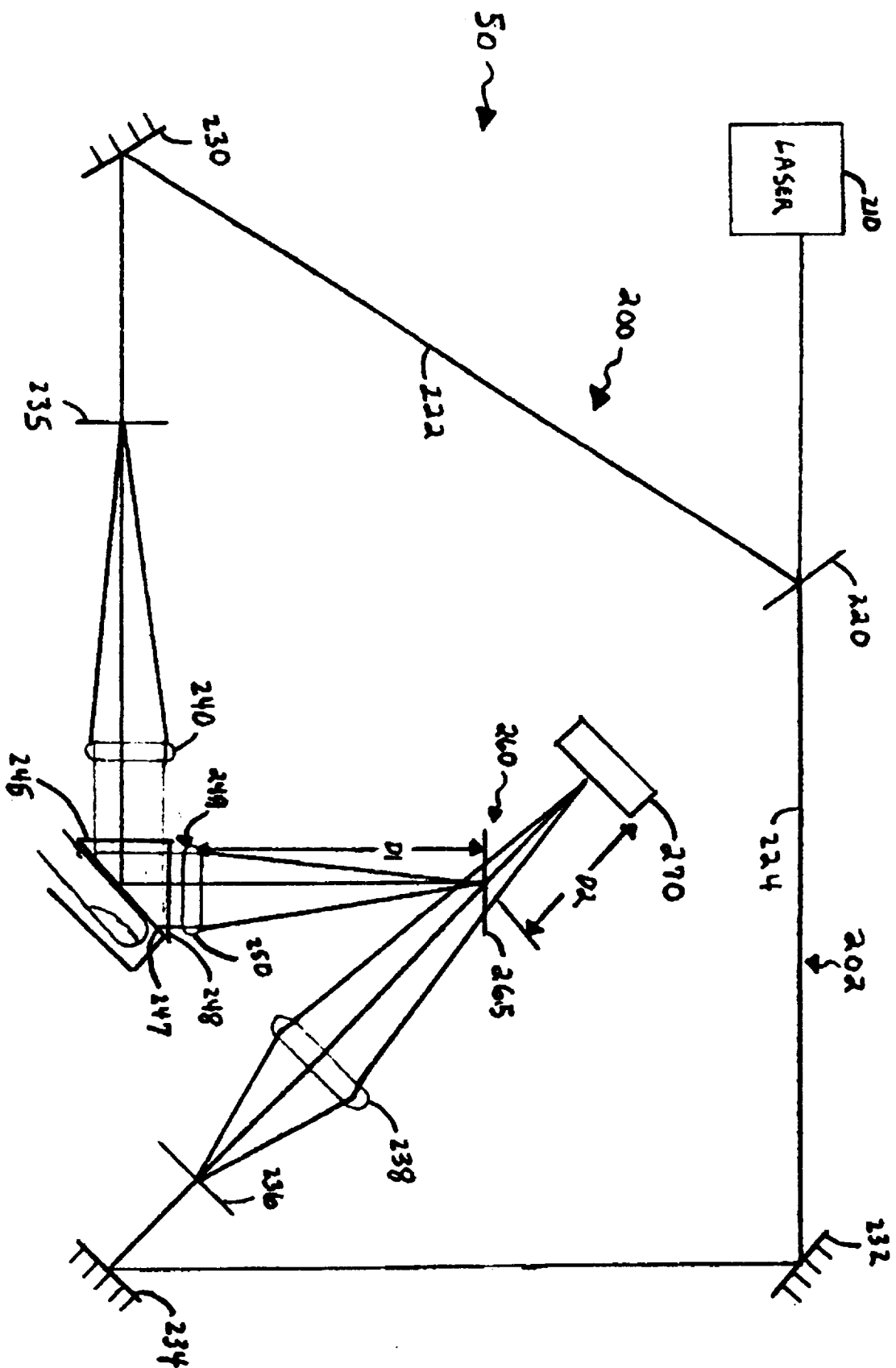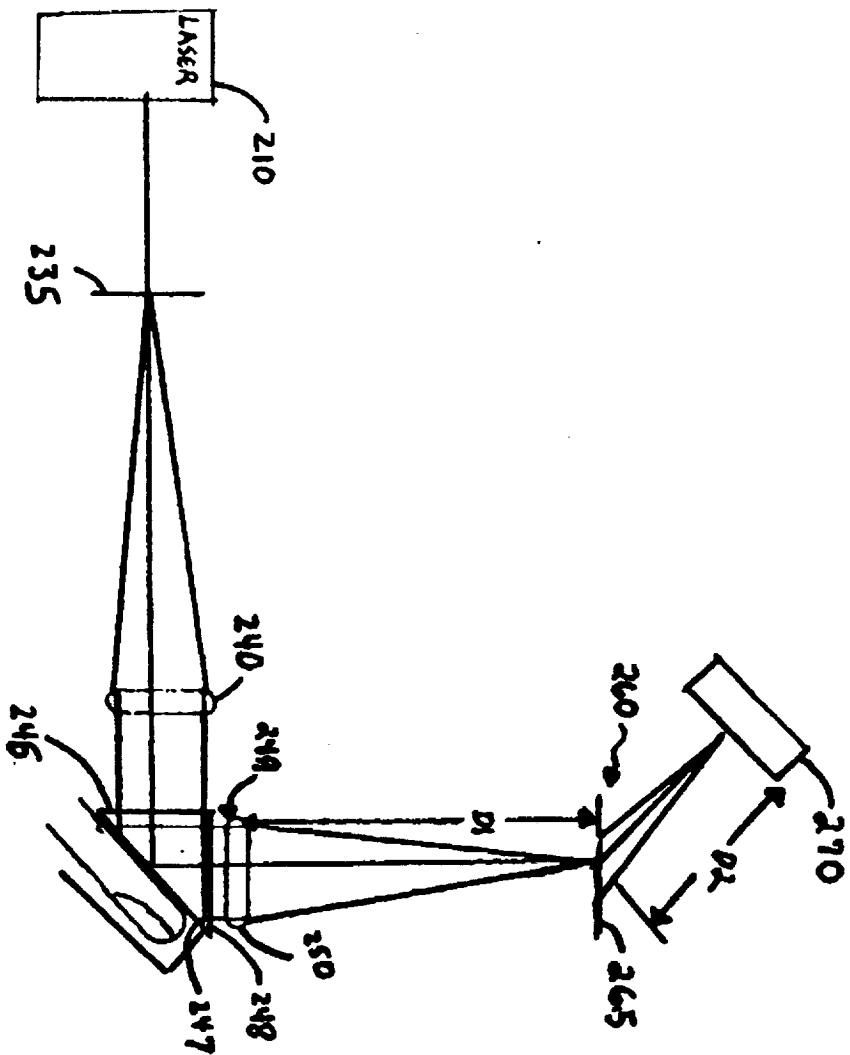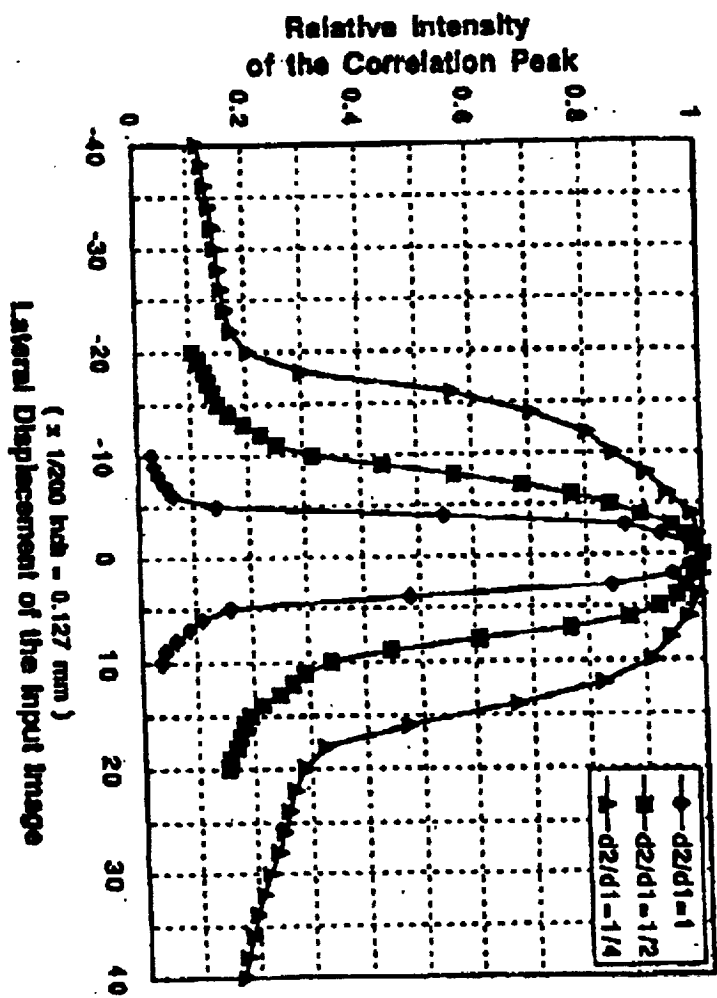
DETECTOR 108

F.G. 2

FIG. 3

FIG. 4

A Large-Capacity Holographic Associative Memory System

Hua-Kuang Liu
Department of Electrical Engineering
University of South Alabama
Mobile, Alabama 36688-0002

Yahong Jin
Department of Electrical and Computer Engineering
University of California at Santa Barbara
Santa Barbara, CA 93106

and

Neville I. Marzwell
Jet Propulsion Laboratory
California Institute of Technology
Pasadena, California 91109-8099

Abstract: The concept of a multi-stage holographic optical random-access memory (HORAM) system is described. The multi-stage HORAM can be used for high-capacity storage and high-speed random retrieval of information. The input to the system may be of the form of pairs of images that are arranged in such a way that joint Fourier transforms can be recorded at the output plane which has a large array of different joint transforms. Associative memory and retrieval can be made based on the principle of inner-product neural net. The spatial multiplexed, instead of angular multiplexed, architecture allows parallel information retrieval without any moving part. A two-stage HORAM, using a Dammann grating and a multi-focus holographic lens, capable of storing 2000 holographic matched filters of input images is used to demonstrate the feasibility of the technique. The multi-stage technique can also be applied to many-to-many free-space interconnections with capability greater than that of a single-stage method. This randomly adaptive and dynamic interconnection technique is useful for a variety of optical neural computing and pattern recognition applications.

1. Introduction

In information management and analysis, parameters such as communication delays, limited resources, and inaccessibility of human manipulation require more intelligent, compact, low-power, and light-weight information management and data storage techniques[1,2]. Among the various new and innovative techniques being developed, 3-D volume holographic memory has been considered important and promising for data storage[3-11]. In this letter, we report, for the first time, a multi-stage holographic optical random-access memory (HORAM) system. The multi-stage HORAM can be used for high-capacity storage and high-speed random retrieval of information suitable for a variety of neural computation and pattern recognition applications. The input to the system may be of the form of pairs of images that are arranged in such a way that joint Fourier transforms can be recorded at the output plane which has a large array of different joint transforms. Associative memory and retrieval can be made based on the principle of inner-product neural net. The multi-stage HORAM has much greater storage capacity than that of a single-stage multi-channel optical holographic memory and pattern recognition system[12-14].

2. Theoretical Discussion

A block diagram illustrating the concept of a HORAM is shown in Figure 1. The input object information $O(x,y)$ is presented in a two-dimensional image or data format which is illuminated by a collimated laser beam. The input $O(x,y)$ can either be presented with a photo transparency or in real-time by a spatial light modulator, such as a liquid crystal television spatial light modulator (LCTV SLM)[15]. The input is then passed through a number of cascaded stages of holographic optical elements (HOE) and shutter arrays that are represented by the H blocks. For illustration, a two-stage system with blocks H_1 and H_2 is used as an example. The HOE in H_1 replicates $O(x,y)$ into an array of $h_1 \cdot h_1$ identical $O(x,y)$'s. The shutter array in H_1 may be electronically controlled such that it can let any number of the $h_1 \cdot h_1$ replica of $O(x,y)$ pass through and stop the others. A multi-focus holographic lens[16] with $h_2 \cdot h_2$ foci may be used for the subsequent H_2 block. A second shutter array may be used to select one of the foci of the multi-focus lens. In the recording of the matched filter at plane F, which is the output of the block H_2, $(h_1 \cdot h_2)^2$ Fourier transforms of $O(x,y)$ will be selected one at a time by the opening of one of each of the switches of the two shutter arrays. Meanwhile, a reference beam is applied to interfere with the Fourier transform for the recording of the holographic

matched filter. By using each Fourier transform in the array to record one of the images or 2-D data, a complete array of matched filters can be recorded. For example, if $h_1=9$ and $h_2=5$, $(9 \cdot 5)^2 = 2,025$ Fourier transforms of $O(x,y)$ can be stored at plane F. If $h_1=33$ and $h_2=7$, and a single matched filter at each focus is recorded, a total of 53,361 Fourier transforms of $O(x,y)$ can be stored at plane F. By randomly switching the shutter in each of the H block to let only one channel of the reference beam pass, the input images or 2-D data become randomly accessible. More details of the H blocks are described below.
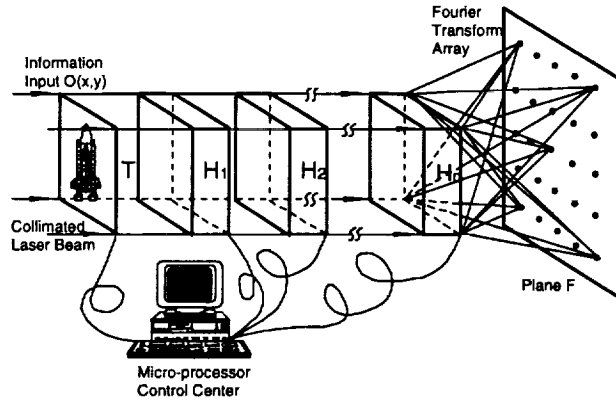
Figure 1.   A concept diagram of a HORAM.

The transmission of the Dammann grating[17, 18] for the block H_1 can be described by

$$t(x,y) = \left[comb\left(\frac{x}{\Delta_d}, \frac{y}{\Delta_d} \right) * g(x,y) \right] a(x,y) , \quad (1)$$

where $comb(x,y)$ represents a comb function[19], the symbol * indicates convolution, Δ_d is the period of the grating, $g(x,y)$ is the shape of the individual groove of the grating, and $a(x,y)$ is the aperture which in general is the incident Gaussian profile of the laser beam. However, for simplicity, the aperture is assumed to be open so that $a(x,y)=1$. The Fourier transform of the grating then becomes

$$T(f_x,f_y) = \Delta_d^2 \left[comb(\Delta_d f_x, \Delta_d f_y) \right] G(f_x,f_y)$$

$$= \sum_{m=-\infty}^{\infty} \sum_{n=-\infty}^{\infty} \delta(f_x - \frac{m}{\Delta_d}) \delta(f_y - \frac{n}{\Delta_d}) \cdot G(f_x,f_y) \quad (2)$$

where $\delta(f_x,f_y)$ is a delta function[19], and $G(f_x, f_y)$ is the Fourier transform of $g(x,y)$. $G(f_x, f_y)$ acts as a window function to attenuate those peaks of $\sum_{m=-\infty}^{\infty} \sum_{n=-\infty}^{\infty} \delta(f_x - \frac{m}{\Delta_d}) \delta(f_y - \frac{n}{\Delta_d})$ that are not wanted,

for a $(2M+1) \cdot (2M+1)$ array, we may design the grating in such a manner that ideally

$$G(f_x,f_y) = \begin{cases} 1 & |m|,|n| \leq M \\ 0 & |m|,|n| > M \end{cases} \quad (3)$$

With Eq. (3), Eq. (2) can be expressed as

$$T(f_x,f_y) = \sum_{m=-M}^{M} \sum_{n=-M}^{M} \delta(f_x - \frac{m}{\Delta_d}) \delta(f_y - \frac{n}{\Delta_d}) . \quad (4)$$

A traditional single-lens Dammann grating Fourier transform system is shown in Figure 2.
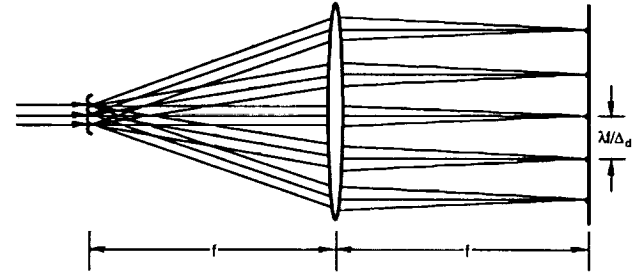

Figure 2.   Diffraction of light passing through a Dammann grating and a lens.

A multi-focus hololens[16] with its architecture and functionality as shown in Figure 3 may be used as the HOE in the block H_2. The multi-focus hololens can be used to produce an array of Fourier transforms of the same input image. When the input is an image carried by a collimated laser beam, the multi-focus hololens will produce at its focal plane an array of replicated Fourier transforms of the input. When one of the foci passes through a selection array spatial filter, it may be reimaged at the output plane.
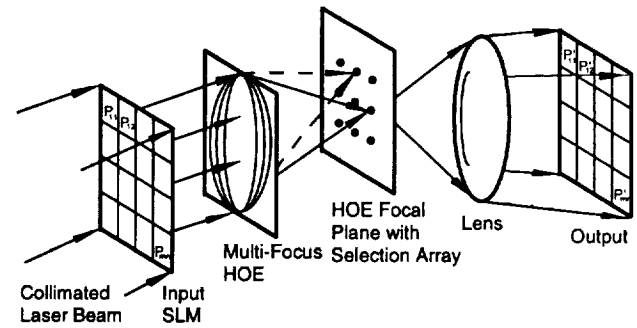

Figure 3.   The architecture and functionality of the multi-focus hololens.

Figure 4 shows an experimental diagram of a two-stage HORAM as described above. A laser beam from an Argon ion laser is divided into an object beam and a reference beam by a beam splitter. The object beam is collimated by a spatial filter and lens L_1 combination.

The collimated beam is used to illuminate the Dammann grating and the input image of an object. A lens L_2 is used to Fourier transform the grating-multiplied object into a $(2M+1) \cdot (2M+1)$ Fourier transform pattern array at the focal plane of L_2, where the shutter array 1 is placed to selectively let one order pass. The input pattern carried by the single diffraction order is collimated by L_3 and passed through the multi-focus lens. It is Fourier-transformed into a $(2N+1) \cdot (2N+1)$ foci array at the focal plane of the hololens. At the focal plane, the shutter array 2 is placed to selectively let one order to pass for recording. Lenses L_4 and L_5 are used to re-image the passed Fourier transform where a holographic matched filter can be recorded.
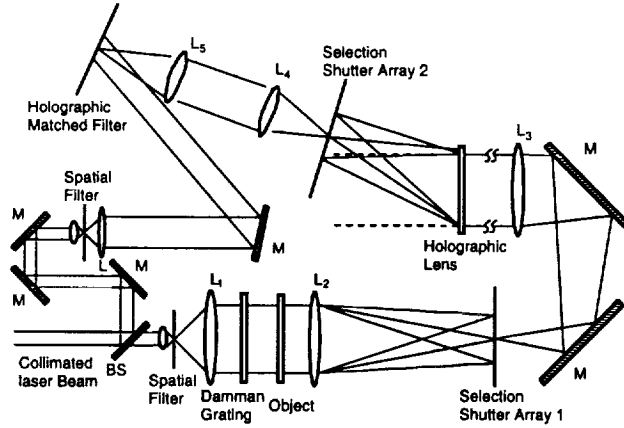

Figure 4. The experimental setup of a HORAM system utilizing the cascade of a Dammann Grating and a multi-focus hololens.

In the recording process, the reference beam is collimated by a spatial filter and lens L combination and is used to interfere with the Fourier transform of the object beam at the matched filter plane. One by one, a total of $(2M+1)^2 \cdot (2N+1)^2$ array of the input data can be stored at the focal plane of L_5, the holographic matched filter plane.

In analysis, as the object in Figure 4 is illumined by an array of beams diffracted by the Dammann grating, the overall transmittance may be described as $t(x,y)O(x,y)$, where $t(x,y)$ and $O(x,y)$ are the transmittance functions of the Dammann grating and the object respectively. Based on Fourier analysis[19] involving the consideration of all elements in the system, a single Fourier transform of the input selected according to the method described at the holographic matched filter plane may be represented by

$$U_m(x_m, y_m)$$

$$= -jA(\lambda f_2)(\lambda f_3)(\lambda f_h)^3 \bar{O}(\frac{f_3}{\lambda f_2 f_h} x_m + \frac{f_3}{f_2 \Delta_h} m_2 - \frac{1}{\Delta_d} m_1,$$

$$\frac{f_3}{\lambda f_2 f_h} y_m + \frac{f_3}{f_2 \Delta_h} n_2 - \frac{1}{\Delta_d} n_1), \qquad (5)$$

where f_2 represents the focal length of lens L_2, f_3 represents the focal length of lens L_3, f_4 and f_5 of lenses L_4 and L_5 are identical and naturally eliminated, f_h represents the focal length of the hololens, $1/\bullet_d$ is the period of the Dammann Grating in the frequency domain, $1/\bullet_h$ is the period of the holographic lens in the frequency domain, (m_1, n_1) is the diffraction order selected from Dammann grating with m_1, n_1 range from $-M$ to M, (m_2, n_2) is the diffraction order selected from the holographic lens with m_2, n_2 range from $-N$ to N, $\bullet$ is the wavelength of the laser, A is a constant associated with the collimated laser input wave amplitude, and $\bar{O}(f_x, f_y)$ is the Fourier transform of the object

$$\bar{O}(f_x, f_y) = F\{O(x, y)\} = \iint O(x, y) \exp[-j2\pi(f_x x + f_y y)] dx dy.$$

3. Feasibility Demonstration

To show the feasibility of the HORAM, an experiment using the diagram shown in Figure 4 was performed. In the experiment, we used a Dammann grating with M=4 (2M+1=9) and a 25-foci hololens with N=2 (2N+1=5). A 25-mW Spectra Physics Model 124B He-Ne laser was used as the input laser source. Focal length of the lenses used in the system are f_1=10 cm, f_2=20 cm, f_3=f_4=f_5=38 cm with corresponding apertures of 4 cm, and 5 cm for L_1 and L_2 respectively. The aperture for the SORL lenses L_3, L_4, and L_5 is 7.6 cm, and the focal length of the hololens f_h=25.4 cm. The effective aperture used for the input image is about 2 mm. The experimental output of the HORAM at plane F of Figure 4 is shown in Figure 5. A total of 2,025 Fourier transforms in a 2-D array of a 45•45 foci array have been obtained in an area of 2 cm by 5 cm at the matched filter plane. Matched filters at a single focus and several randomly selected foci have been conventionally recorded and the correlation signals have been observed.
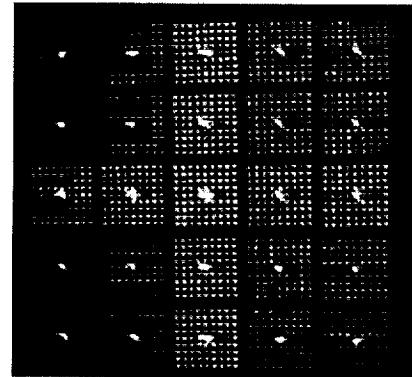

Figure 5. Experimental demonstration: a 2025-channel (45•45) Fourier transform array at the matched filter plane in Figure 4 of a 2-stage optical RAM.

4. Conclusion

In conclusion, we have described a new technique of using multiple stages of free-space interconnection holographic elements to implement a HORAM. We have demonstrated the technique with the memory capacity of over 2000 images. Potentially, tens of thousands of images can be stored. Micro-processors may be used to obtain fast random access to any data set from the memory. An advantage of this technique is that, unlike the angular multiplexed storage method, there is no need of moving any component in the system. High-speed access is therefore achievable. Each of the thousands of Fourier transforms in the array may be used to record a matched filter of an input image of 256•256, 512•512 or any other number of pixels. Therefore, with the HORAM, ultra-high speed special-purpose computing goals can be achieved. For example, simultaneous optical pattern recognition and/or data processing of the super-large array at 1 microsecond means a computing speed on the order of $1.2 \cdot 10^{16}$ bits/sec assuming that binary images are used. If the finger prints of criminals are stored in the memory, the HORAM can determine whether an arbitrary input finger print belongs to one of the criminals. The recognition can be accomplished remotely and the HORAM can make instantaneous decisions.

The multi-stage architecture can also be applied to many-to-many free-space interconnections with each input pixel reconfigurably connectable to any number of the output foci. The interconnection capability should be much higher than that of any other single-stage free-space optical interconnection method reported[17]. This randomly adaptive and dynamic interconnection technique is useful for a variety of optical neural computing and optical pattern recognition applications.

Acknowledgment

References

1. B. J. Goertzen and P. A. Mitkas, Opt. Eng., **35**(7), 1847 (1996).
2. P. B. Berra, A. Ghafoor, P. A. Mitkas, S. J. Marcinkowski, and M. Guizani, IEEE Trans. Knowledge Data Eng., **11**, 111 (1989).
3. N. V. Kukhtarev, V. B. Markov, S. G. Odulov, M. S. Soskin, and V. L. Vinetskii, Ferroelectrics, **22**, 949 (1979).
4. J. F. Heanue, M. C. Bashaw, and L. Hesselink, Science, **265**(5173), 749 (1994).
5. F. H. Mok, Opt. Lett., **18**, 915 (1993).
6. S. Yin, H. Zhou, F. Zhao, M. Wen, Z. Yang, and F. T. S. Yu, Opt. Comm., **101**, 317 (1993).
7. P. A. Mitkas and L. J. Irakliotis, J. Opt. Memories Neural Net., 3(2), 87 (1994).
8. J. H. Hong, I. McMichael, T. Y. Chang, W. Christian, and E. G. Paek, Opt. Eng. **34**(8), 2193 (1992).
9 D. Psaltis, Byte, **17**(9), 179 (1995).
10. J. R. Wullert II and Y. Lu, Appl. Opt., **33**(11), 3192 (1994).
11. F. T. S. Yu and S. Yin, Optical Memory Neural Networks, **3**, 207 (1994).
12. D. Gregory, G. Duthie, and H. K. Liu, Appl. Opt., **23**, 4560-4570 (1984).
13. H. K. Liu, J. Barhen, and N. Farhat, U. S. Patent No 5,544,280, issued on August 6, 1996
14. H. K. Liu and J. Wu, Appl. Opt., **31**, 4631 (1992)
15. H. K. Liu and T. H. Chao, Appl. Opt., **28**, 4772 (1989).
16. Y. Z. Liang, D. Z. Zhao, and H. K. Liu, Appl. Opt., **22**, 3451 (1983).
17. H. Dammann and K. Grotler, Opt. Comm., **3**, 312 (1971)
18. M. Blume, F. B. McCormick, P. J. Marchand, and S. C. Esener, Proc. SPIE, **5537**, 180 (1995).
19. J. W. Goodman, Introduction to Fourier Optics, McGraw-Hill, (1968).

Advanced ultra-high-capacity optical random access memory and pattern recognition techniques

Hua-Kuang Liu, FELLOW SPIE
Yahong Jin, MEMBER SPIE
University of South Alabama
Department of Electrical and Computer
 Engineering
Mobile, Alabama 36688-0002
E-mail: hkliu@jaguar1.usouthal.edu

Neville I. Marzwell
California Institute of Technology
Jet Propulsion Laboratory
Pasadena, California 91109-8099

Abstract. The architecture and mathematical analysis of a new multi-channel multistage holographic optical random access memory (HORAM) architecture and an experimental demonstration of its feasibility are presented. The new HORAM can be used for ultra-high-capacity storage and high-speed random retrieval of information. A two-stage HORAM, using a Dammann grating and a multifocus holographic lens, clearly shows the capability of storing 2000 holographic matched filters. The functional requirements for key optical elements including laser sources, spatial light modulators, and electro-optical shutters for making a desired practical and compact HORAM are described. The potential extension of the HORAM system for multiple-channel optical pattern recognition, classification, and image restoration are described. © *1998 Society of Photo-Optical Instrumentation Engineers.* [S0091-3286(98)02503-3]

1 Introduction

Instruments with high speed and large capacity *in situ* data identification, classification, and storage capabilities are required for information management and analysis. For example, in National Aeronautics and Space Administration (NASA) applications, extremely large volumes of data sets must processed in space exploration, space habitation and utilization, and in various missions to planet-earth programs. Parameters such as communication delays, limited resources, and inaccessibility of human manipulation require more intelligent, compact, low-power, and light-weight information management and data storage techniques.[1,2] For this reason, new and innovative techniques are being developed by many researchers in the field. Among the various techniques being developed, the 3-D volume holographic memory has been considered as one of the most important and promising for data storage.[3-11] For example, Mok[5] reported that more than thousands of holograms can be stored in a lithium niobate crystal via angular multiplexing, Heanue et al.[4] demonstrated the storage and retrieval of digital data using a volume hologram, and Yu and Yin have used a volume photorefractive crystal to make a reflection type matched filter applicable for pattern recognition.[11] The purpose of this paper is to present a new and basic concept of a multichannel multistage spatially parallel holographic optical random access memory (HORAM) system and the theoretical analysis of a two-stage HORAM architecture. The preliminary experimental results demonstrating the storage plane of a 2000-channel system and its potential for optical pattern recognition are presented. We then present various optical computing methods based on the HORAM architecture. The multistage HORAM can be used for the storage

and random information retrieval among an extremely large amount of data and a family of pattern recognition applications. Advantages of the HORAM include large data storage capacity and high-speed parallel retrieval without moving parts. For a two-stage HORAM, two orders of magnitude of increment of the storage capacity can be achieved as compared with that of the single-staged spatial multiplexed multichannel optical pattern recognition system previously reported.[12-14] The practical limitations of the new architecture, primarily due to the availability of some basic components, are described at the end of the paper to stimulate further technology innovation and advancement required for this important technique.

2 Theoretical Discussion

The basic concept of the HORAM is shown in Fig. 1, where the input information T is presented in a 2-D image or data format, which is carried by a collimated laser beam. The input can either be presented with a phototransparency or in real time by a spatial light modulator. An example of an inexpensive laboratory type electronically addressed spatial light modulator is the liquid crystal television spatial light modulator[15] (LCTV SLM). The input T is then applied through a multiple number of cascaded stages of holographic optical elements (HOEs) and shutter arrays that are represented by the H blocks. Each H block may contain HOEs and shutter arrays. The functions of these elements are described by using blocks H_1 and H_2 as examples. The HOE in H_1 replicates input T into an array of $h_1 \times h_1$ identical T's. The shutter array in H_1 can be electronically controlled such that it can let any one of the $(h_1)^2$ replicas of T pass through and stop the others. The subsequent H_2 block
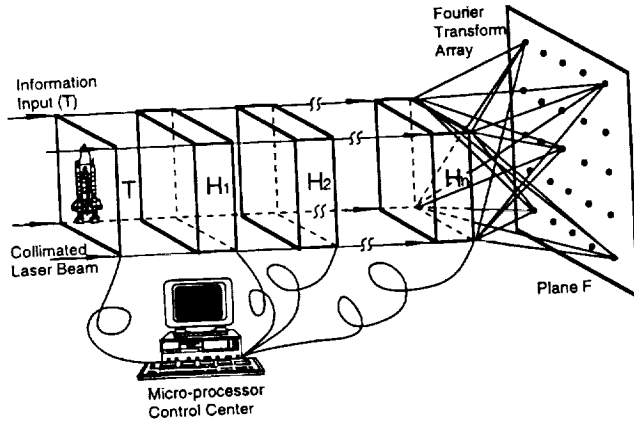
Fig. 1 Block diagram illustrating the concept of a HORAM.

Fig. 2 Diffraction of light passing through a Dammann grating and a lens.

has the function of a multifocus holographic lens with $(h_2)^2$ foci. A second shutter array can be used to select one of the foci of the multifocus lens. Hence at the output of the block H_2, $(h_1 \times h_2)^2$ Fourier transforms of T will appear one at a time at plane F since each time one of the Fourier transforms is selected, it is accomplished by the opening of one of each of the switches of the two shutter arrays. If one applies a reference beam to interfere with the Fourier transform, a holographic filter can be recorded at plane F. By using each Fourier transform in the array to record one of the images or 2-D data, a complete array of matched filters can be recorded. For example, if two H blocks are used with $h_1 = 9$ and $h_2 = 5$, a minimum of $(9 \times 5)^2 = 2025$ Fourier transforms of T can be stored at plane F if only one Fourier transform is recorded at each point of the array. Since holograms can be superpositioned, if each point is used to record four Fourier transforms by angular multiplexing, over 10,000 matched filters can be recorded at plane F. If $h_1 = 33$ and $h_2 = 7$ and a single matched filter at each focus is recorded, a total of 53,361 Fourier transforms of T can be stored at plane F. In the preceding examples, if the input data are images of human faces, then over 50,000 faces can be memorized in a HORAM. In the pattern recognition process, an input can be used to address all the stored holographic filters and therefore auto- or heterocorrelation signals can be obtained. On the other hand, by switching the shutter in each of the H blocks to let only one channel of the reference beam pass, one of the input images or 2-D data becomes randomly accessible.

One possible implementation of the HORAM in a two-stage architecture is to use a high-efficiency Dammann phase grating[16,17] with a lens and a shutter for H_1, and a multifocus holographic lens[18] (hololens) with a shutter for H_2. The transmission of the Dammann grating can be described as[19]

$$t(x,y) = \left[\text{comb}\left(\frac{x}{L_d}, \frac{y}{L_d} \right) * g(x,y) \right] a(x,y), \qquad (1)$$

where $*$ indicates the convolution operator; L_d is the period of grating; $g(x,y)$ is the shape of the individual groove;
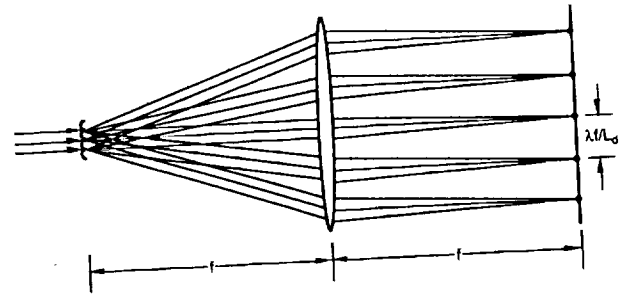
and $a(x,y)$ is the aperture, which in general is the incident Gaussian profile of the laser beam. However, for simplicity, the aperture is assumed to be open and uniform, so that $a(x,y) = 1$. The Fourier transform of the grating[19] is

$$T(f_x, f_y) = L_d^2 [\text{comb}\ (L_d f_x, L_d f_y)] G(f_x, f_y)$$

$$= \sum_{m=-\infty}^{\infty} \sum_{n=-\infty}^{\infty} \delta\left(f_x - \frac{m}{L_d} \right) \delta\left(f_y - \frac{n}{L_d} \right) G(f_x, f_y), \qquad (2)$$

where $G(f_x, f_y)$ is the Fourier transform of $g(x,y)$, and $G(f_x, f_y)$ acts as a window function to attenuate those peaks of $\sum_{m=-\infty}^{\infty} \sum_{n=-\infty}^{\infty} \delta(f_x - m/L_d) \delta(f_y - n/L_d)$ that are not wanted. For a $(2M+1) \times (2M+1)$ array, we design the grating in such a manner that ideally

$$G(f_x, f_y) = \begin{cases} 1 & |m|, |n| \leq M \\ 0 & |m|, |n| > M. \end{cases} \qquad (3)$$

With Eq. (3), Eq. (2) can be expressed as

$$T(f_x, f_y) = \sum_{m=-M}^{M} \sum_{n=-M}^{M} \delta\left(f_x - \frac{m}{L_d} \right) \delta\left(f_y - \frac{n}{L_d} \right). \qquad (4)$$

A traditional single-lens Dammann grating Fourier transform system is shown in Fig. 2.

A multifocus hololens[18] with its architecture and functionality as shown in Fig. 3 can be used as the HOE in H_2.
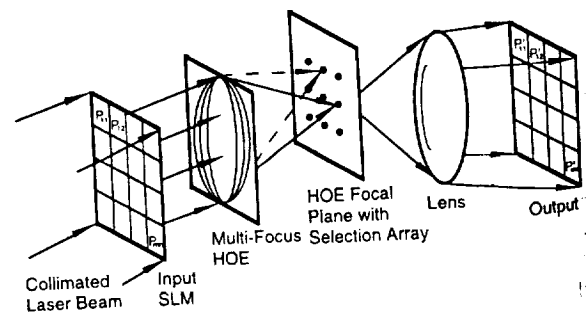

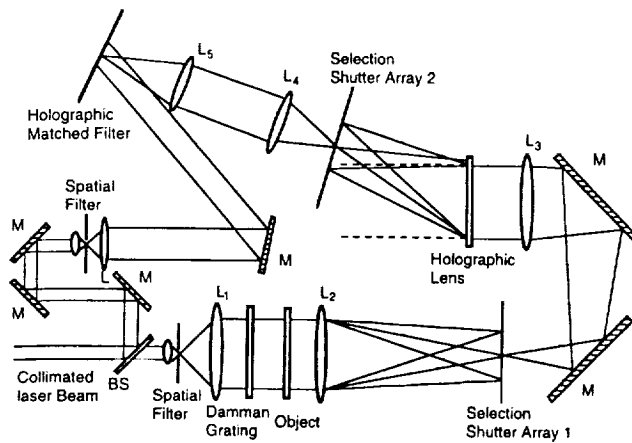**Fig. 3** Architecture and functionality of the multifocus hololens.

Fig. 4 Experimental setup of a HORAM system utilizing the cascade of a Dammann grating and a multifocus hololens.

of Fig. 1. The element was designed via a detailed Fourier computation and diffraction analysis[19] such that it will work as a lens with an array of foci. This multifocus hololens is different from an array of microlenses because the multifocus lens has a single aperture where the array of microlenses form foci, each of which has its own aperture. Therefore the multifocus hololens can be used to produce an array of Fourier transforms of the same input image where a microlens array cannot. For example, if the input to the multifocus hololens is a single laser beam, the beam can be directed to the array of foci with energy divided equally among the foci. When the input is an image carried by the collimated laser beam, in an ideal case, the multifocus hololens will produce at its focal plane an array of replicated Fourier transforms of the input. When one of the foci passes through a selection array spatial filter (in the form of small openings), it can be reimaged at the output plane. Special spectral modulation can be performed at the focal plane and image processing can be performed at the image plane. This architecture is therefore highly versatile. Moreover, by properly cascading the two HOEs as described, one can greatly increase the number of channels that can be processed in parallel. For example, the interconnection capacity and computation speed can hardly competed with by any other method.

The described HOEs can be invoked in an architecture, as shown in Fig. 4, as one way to implement the concept shown in Fig. 1. The architecture utilizes a cascaded combination of a Dammann phase grating and a multifocus hololens. A laser beam from an argon ion laser is divided into an object beam and a reference beam by a beamsplitter (BS). The object beam is collimated by a spatial filter and lens L_1 combination. The collimated beam is used to illuminate the Dammann grating and the input transparency so the output carries the input object. Lens L_2 is used to Fourier transform the object-carrying input beam multiplied by the transmittance of the Dammann grating into a $(2M + 1) \times (2M + 1)$ equal-intensity Fourier transform pattern

array at the focal plane of L_2, where shutter array 1 is placed to selectively let one order pass in the recording process. The input pattern carried by the single diffraction order is imaged by L_3 to pass through the multifocus lens and is then Fourier transformed into the $(2N+1) \times (2N +1)$ foci array at the focal plane of the hololens, where N is the maximum diffraction order of the hololens. At the focal plane, the selection shutter array 2 is placed to selectively let one order to pass. Lenses L_4 and L_5 are used to reimage the passed Fourier transform where a holographic matched filter can be recorded. In the recording process, the reference beam is collimated by a spatial filter and lens L combination and is used to interfere with the Fourier transform of the object beam at the matched filter plane. If one let one object pass at each recording and let the reference beam to interfere only with that order, a total of $(2M + 1)^2 \times (2N+ 1)^2$ array of input data can be stored at the focal plane of L_5, as shown in Fig. 4. The data/image formation property of the HORAM shown in Fig. 4 is described in the following.

2.1 Amplitude Distribution at Plane P_2 (Fourier Transform Plane of L_2)

The object is illumined by an array of beams diffracted by the Dammann grating. The overall transmittance may be described as $t(x,y)O(x,y)$, where $t(x,y)$ and $O(x,y)$ are the transmittance functions of the Dammann grating and the object, respectively. Assuming that the combined grating-object is placed at one focal length in front of lens L_2, the result is an optically Fourier transformed array located at the back focal plane P_2 of L_2. The beam amplitude distribution at P_2 can be represented by a $(2M + 1) \times (2M + 1)$ array of Fourier transform of the object by lens L_2:

$$S_2(f_x, f_y) = \frac{A}{j\lambda f_2} F_2[t(x,y)O(x,y)]$$

$$= \frac{A}{j\lambda f_2} \sum_{m_d=-M}^{M} \sum_{n_d=-M}^{M} \delta\left(f_x - \frac{m_d}{L_d}\right)$$

$$\times \delta\left(f_y - \frac{n_d}{L_d}\right) * F_2[O(x,y)]$$

$$= \frac{A}{j\lambda f_2} \sum_{m_d=-M}^{M} \sum_{n_d=-M}^{M} \delta\left(f_x - \frac{m_d}{L_d}\right)$$

$$\times \delta\left(f_y - \frac{n_d}{L_d}\right) * \tilde{O}(f_x, f_y), \tag{5}$$

where λ is the wavelength of the laser, A is a constant associated with the collimated laser input wave amplitude, f_2 is the focal length of lens L_2. $1/L_d$ is the period of the Dammann Grating in frequency domain, and F_n denotes the Fourier transform by lens $L_n (n = 1,2,...)$,

$$\bar{O}(f_x, f_y) = F_2[O(x,y)]$$

$$= \int \int O(x,y) \exp[-j2\pi(f_x x + f_y y)] \, dx \, dy,$$

$$(6)$$

where f_x and f_y are the spatial frequencies: $f_x = x_2/(\lambda f_2)$ and $f_y = y_2/(\lambda f_2)$; and (x_2, y_2) are points in plane P_2. The amplitude distribution at P_2 can also be expressed in terms of the position at plane P_2:

$$U_2(x_2, y_2) = S_2\left(\frac{x_2}{\lambda f_2}, \frac{y_2}{\lambda f_2}\right)$$

$$= \frac{A(\lambda f_2)^2}{j(\lambda f_2)} \sum_{m_d=-M}^{M} \sum_{n_d=-M}^{M} \delta\left(x_2 - \frac{\lambda f_2}{L_d} m_d\right)$$

$$\times \delta\left(y_2 - \frac{\lambda f_2}{L_d} n_d\right) * \bar{O}\left(\frac{x_2}{\lambda f_2}, \frac{y_2}{\lambda f_2}\right)$$

$$= \frac{A}{j(\lambda f_2)} M_d(x_2, y_2) * \bar{O}\left(\frac{x_2}{\lambda f_2}, \frac{y_2}{\lambda f_2}\right), \quad (7)$$

where

$$M_d(x_2, y_2) = (\lambda f_2)^2 \sum_{m_d=-M}^{M} \sum_{n_d=-M}^{M} \delta\left(x_2 - \frac{\lambda f_2}{L_d} m_d\right)$$

$$\times \delta\left(y_2 - \frac{\lambda f_2}{L_d} n_d\right). \quad (8)$$

An aperture can be placed at plane P_2 with a selection filter, which is set to select one of the $(2M+1) \times (2M+1)$ equal-intensity diffraction orders.

2.2 Amplitude Distribution at Fourier Plane of Lens L_3

Lens L_3 is placed at distance f_3 from plane P_2. Due to the input at plane P_2, the amplitude distribution at the Fourier plane of lens L_3 can be written as

$$S_3(f_{x_2}, f_{y_2}) = \frac{1}{j\lambda f_3} F_3[U_2(x_2, y_2)]$$

$$= -\frac{A}{(\lambda f_2)(\lambda f_3)} F_3\{M_d(x_2, y_2) * F_2[O(x,y)]\}$$

$$= -\frac{A}{(\lambda f_2)(\lambda f_3)} F_3[M_d(x_2, y_2)]$$

$$\times F_3 F_2[O(x,y)]. \quad (9)$$

The amplitude distribution Eq. (9) can also be expressed in terms of the position at Fourier plane of lens L_3, that is

$$U_3(x_3, y_3) = S_3\left(\frac{x_3}{\lambda f_3}, \frac{y_3}{\lambda f_3}\right)$$

$$= -\frac{A(\lambda f_2)^2}{(\lambda f_2)(\lambda f_3)} \bar{M}_d\left(\frac{x_3}{\lambda f_3}, \frac{y_3}{\lambda f_3}\right)$$

$$\times O\left(-\frac{f_2}{f_3} x_3, -\frac{f_2}{f_3} y_3\right), \quad (10)$$

where

$$\bar{M}_d(f_x, f_y) = F_3\{M_d(x,y)\}.$$

2.3 Amplitude Distribution at the Fourier Plane of the Holographic Lens

The holographic lens Fourier transforms the input $U_3(x_3, y_3)$ to a $(2N+1) \times (2N+1)$ array of spectrum onto its Fourier transform plane. The amplitude distribution is

$$S_h(f_{x_3}, f_{y_3})$$

$$= \frac{1}{j\lambda f_h} \sum_{m_h=-N}^{N} \sum_{n_h=-N}^{N} \delta\left(f_{x_3} - \frac{m_h}{L_h}\right) \delta\left(f_{y_3} - \frac{n_h}{L_h}\right)$$

$$* F_h[U_3(x_3, y_3)]$$

$$= -\frac{A(\lambda f_2)^2}{j(\lambda f_2)(\lambda f_3)(\lambda f_h)}$$

$$\times \sum_{m_h=-N}^{N} \sum_{n_h=-N}^{N} \delta\left(f_{x_3} - \frac{m_h}{L_h}\right) \delta\left(f_{y_3} - \frac{n_h}{L_h}\right)$$

$$* F_h\left[\bar{M}_d\left(\frac{x_3}{\lambda f_3}, \frac{y_3}{\lambda f_3}\right)\right] * F_h\left[O\left(-\frac{f_2}{f_3} x_3, -\frac{f_2}{f_3} y_3\right)\right]$$

$$= -\frac{A}{j(\lambda f_2)(\lambda f_3)(\lambda f_h)}$$

$$\times \sum_{m_h=-N}^{N} \sum_{n_h=-N}^{N} \delta\left(f_{x_3} - \frac{m_h}{L_h}\right) \delta\left(f_{y_3} - \frac{n_h}{L_h}\right)$$

$$* F_h F_3[M_d(x_2, y_2)] * F_h F_3\left[\bar{O}\left(\frac{x_2}{\lambda f_2}, \frac{y_2}{\lambda f_2}\right)\right]. \quad (11)$$

The amplitude distribution [Eq. (11)] can also be expressed in terms of the position at the Fourier plane of the holographic lens, that is

$$U_h(x_h, y_h)$$

$$= S_3\left(\frac{x_h}{\lambda f_h}, \frac{y_h}{\lambda f_h}\right)$$

$$= -\frac{A(\lambda f_3)^4(\lambda f_h)^2}{j(\lambda f_2)(\lambda f_3)(\lambda f_h)}$$

$$\times \sum_{m_h=-N}^{N}\sum_{n_h=-N}^{N}\delta\left(x_h-\frac{\lambda f_h}{L_h}m_h\right)\delta\left(y_h-\frac{\lambda f_h}{L_h}n_h\right)$$

$$*M_d\left(-\frac{f_3}{f_h}x_h,-\frac{f_3}{f_h}y_h\right)*\tilde{O}\left(-\frac{f_3}{\lambda f_2 f_h}x_h,\right.$$

$$\left.-\frac{f_3}{\lambda f_2 f_h}y_h\right)$$

$$= -\frac{A(\lambda f_3)^4}{j(\lambda f_2)(\lambda f_3)(\lambda f_h)}M_h(x_h,y_h)$$

$$*M_d\left(-\frac{f_3}{f_h}x_h,-\frac{f_3}{f_h}y_h\right)*\tilde{O}\left(-\frac{f_3}{\lambda f_2 f_h}x_h,\right.$$

$$\left.-\frac{f_3}{\lambda f_2 f_h}y_h\right),\tag{12}$$

where f_h is the focal length of the holographic lens, $1/L_h$ is the period of the holographic lens in the frequency domain, and

$$M_h(x_h,y_h)=(\lambda f_h)^2\sum_{m_h=-N}^{N}\sum_{n_h=-N}^{N}\delta\left(x_h-\frac{\lambda f_h}{L_h}m_h\right)$$

$$\times \delta\left(y_h-\frac{\lambda f_h}{L_h}n_h\right).\tag{13}$$

2.4 Light Amplitude Distribution at the Matched Filter Plane

For simplicity, L_4 and L_5 are selected as a pair of lenses with the same focal length f_4. Lens L_4 is placed at a distance f_4 from the Fourier plane of the holographic lens and lens L_5 is placed $2f_4$ from lens L_4. The matched filter plane is at the focal plane of lens L_5. The amplitude distribution at the matched filter plane can be expressed as

$$U_m(x_m,y_m)=-\frac{1}{(\lambda f_4)^2}F_5F_4[U_h(x_h,y_h)]$$

$$=-U_h\left(-\frac{f_4}{f_5}x_m,-\frac{f_4}{f_5}y_m\right).\tag{14}$$

Since $f_4=f_5$, we have

$$U_m(x_m,y_m)=-U_h(-x_m,-y_m)$$

$$=\frac{A(\lambda f_3)^4}{j(\lambda f_2)(\lambda f_3)(\lambda f_h)}M_h(-x_m,-y_m)$$

$$*M_d\left(\frac{f_3}{f_h}x_m,\frac{f_3}{f_h}y_m\right)$$

$$*\tilde{O}\left(\frac{f_3}{\lambda f_2 f_h}x_m,\frac{f_3}{\lambda f_2 f_h}y_m\right),\tag{15}$$

where (x_m,y_m) is a point at the matched filter plane. It can be seen that the amplitude distribution at the matched filter plane is proportional to a $(N\times N)$ with $(M\times M)$ array of the Fourier transforms of the object

$$\tilde{O}(f_x,f_y)=F[O(x,y)]$$

$$=\int\int O(x,y)\exp[-j2\pi(f_x x+f_y y)]\,dx\,dy,$$

where

$$f_x=\frac{f_3}{\lambda f_2 f_h}x_m \quad \text{and} \quad f_y=\frac{f_3}{\lambda f_2 f_h}y_m.$$

2.5 Recording of the Holographic Matched Filter

In the recording of the holographic matched filter, two selection shutter arrays are placed at the plane P_2 and at the Fourier plane of the holographic lens, respectively. The shutter arrays are set such that only one order each from the Dammann grating and the holographic lens is selected to pass. Once the order (m_1,n_1) from Dammann grating and the order (m_2,n_2) from holographic lens are selected, the amplitude distribution at the matched filter plane, or Eq. (15), becomes

$$U_m(x_m,y_m)=\frac{A(\lambda f_2)^2(\lambda f_3)^4(\lambda f_h)^2}{j(\lambda f_2)(\lambda f_3)(\lambda f_h)}\delta\left(-x_m-\frac{\lambda f_h}{L_h}m_2\right)$$

$$\times \delta\left(-y_m-\frac{\lambda f_h}{L_h}n_2\right)*\delta\left(\frac{f_3}{f_h}x_m-\frac{\lambda f_2}{L_d}m_1\right)$$

$$\times \delta\left(\frac{f_3}{f_h}y_m-\frac{\lambda f_2}{L_d}n_1\right)$$

$$*\tilde{O}\left(\frac{f_3}{\lambda f_2 f_h}x_m,\frac{f_3}{\lambda f_2 f_h}y_m\right)$$

$$=-jA(\lambda f_2)(\lambda f_3)(\lambda f_h)^3\delta\left(-x_m-\frac{\lambda f_h}{L_h}m_2\right)$$

$$\times \delta\left(-y_m-\frac{\lambda f_h}{L_h}n_2\right)*\delta\left(x_m-\frac{\lambda f_2 f_h}{f_3 L_d}m_1\right)$$

$$\times \delta\left(y_m-\frac{\lambda f_2 f_h}{f_3 L_d}n_1\right)$$

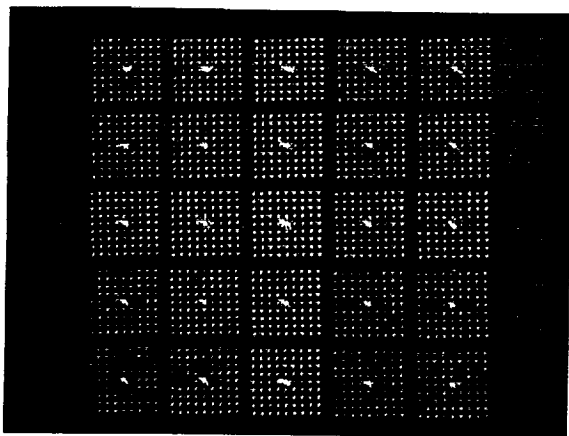$$*\tilde{O}\left(\frac{f_3}{\lambda f_2 f_h}x_m,\frac{f_3}{\lambda f_2 f_h}y_m\right),\tag{16}$$

or

Fig. 5 Experimental demonstration: a 2025-channel (45×45) Fourier transform array at the plane F in Fig. 1 of a two-stage optical RAM.

$$U_m(x_m, y_m) = -jA(\lambda f_2)(\lambda f_3)(\lambda f_h)^3 \bar{O}\left(\frac{f_3}{\lambda f_2 f_h} x_m\right.$$

$$+ \frac{f_3}{f_2 L_h} m_2 - \frac{1}{L_d} m_1, \frac{f_3}{\lambda f_2 f_h} y_m + \frac{f_3}{f_2 L_h} n_2$$

$$\left. - \frac{1}{L_d} n_1\right), \tag{17}$$

where m_1 and n_1 range from $-M$ to M and m_2 and n_2 range from $-N$ to N. Once (m_1, n_1) and (m_2, n_2) are selected by shutter arrays 1 and 2, only one Fourier transform of the input image is recorded at matched filter plane. From this analysis, we can see that the total number of channels of the system is determined by the Dammann grating and the holographic lens used.

3 Experimental Demonstration

To show the feasibility of the HORAM, a preliminary experiment using the configuration shown in Fig. 4 was performed. In the experiment, we used a Dammann grating with $M=4$ ($2M+1=9$) and a 25-foci hololens with $N=2(2N+1=5)$. A 25-mW Spectra Physics Model 164 He-Ne laser was used as the input laser source. Focal length of the lenses used in the system are $f_1 = 10$ cm, $f_2 = 20$ cm, and $f_3 = f_4 = f_5 = 38$ cm with corresponding apertures of 4 and 5 cm for L_1 and L_2 respectively, and 7.62 cm for the SORL lenses L_3, L_4, and L_5, the focal length of the hololens $f_h = 25.4$ cm. The effective aperture used for the input image is about 5 mm. The experimental output of a two-stage HORAM at the mulplexed Fourier transform array output plane of Fig. 4 is shown in Fig. 5. A total of 2025 Fourier transforms in a 2-D array of 45×45 foci format has been obtained in an area of 2×2 cm at the matched filter plane. Matched filters at a single focus and several randomly selected focuses have been recorded and the correlation signals have been observed.
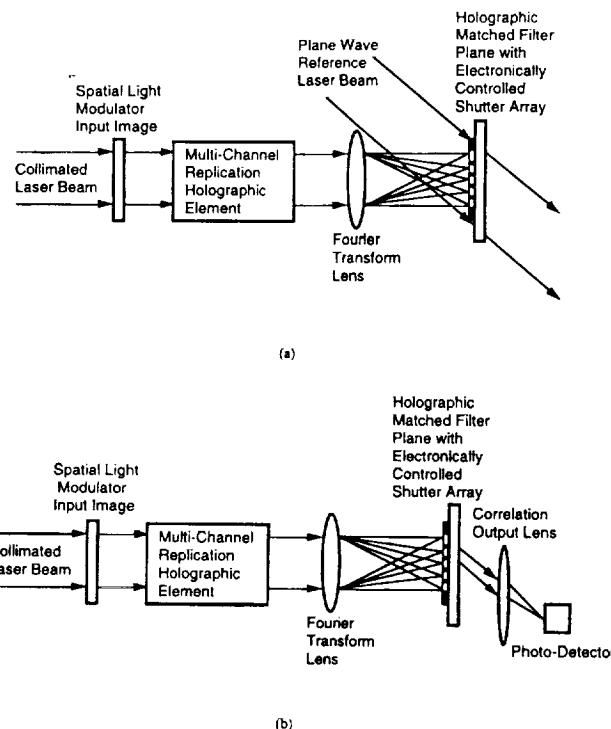

(a)

(b)

Fig. 6 (a) Multichannel pattern recognition system reording architecture and (b) multichannel pattern recognition system addressing architecture.

## 4 Optical Pattern Recognition and Computing Methods Based on the HORAM

The HORAM has a broad range of applications. Based on the multistage HORAM architecture, a few optical pattern recognition and special-purpose optical computing methods can be implemented as described next.

4.1 Multichannel Pattern Recognition System

The recording and addressing architecture of a multichannel pattern recognition system are shown, respectively, in Figs. 6(a) and 6(b). In Fig. 6(a), the object is presented to the system via a spatial light modulator illuminated by a collimated laser beam. The image is replicated in a similar manner as that in the HORAM as described. The replicated images form an array of Fourier transform patterns at the holographic matched filter plan where the matched filters can be made by using a single plane reference wave during the image storage process. For each image, a shutter is open to select one of the Fourier transform of the array. In the addressing process, if an input object image is one of the images stored, the output correlation signal will immediately reveal the answer. To give a numerical example, if the same image is rotated five times and stored in the same location of a matched filter, an array of 2000 would enable 10,000 images to be stored. The capacity of storage would allow recognition of images with rotation and scale variations.

4.2 Multichannel Pattern Classification System

The recording and addressing architecture of a multichannel pattern classification system are shown, respectively, in

(a)

(b)
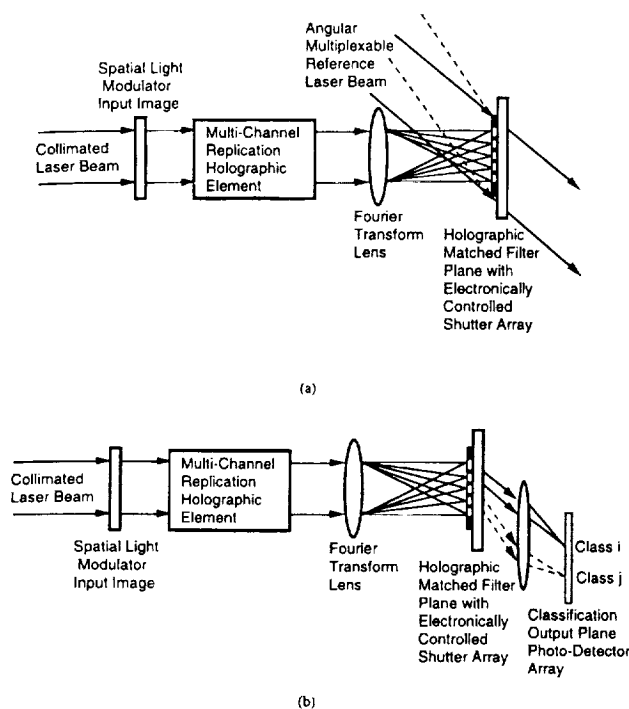
Fig. 7 (a) Multichannel pattern classification system recording architecture and (b) multichannel pattern classification system reording architecture.

Figs. 7(a) and 7(b). The recording and addressing processes are similar to those described in Sec. 4.1. The major difference is that in this case, an orientation variable plane wave is used for the image storage process. The images or features belong to the same class is stored with a certain selected orientation of the reference beam. In the addressing process, if an input object image is one of the class of the images stored, the position of the output correlation signal will immediately reveal the class that the image belongs to. For example, the 10,000 images of the example given in Sec. 4.1 can be classified into 100 classes by using 100 reference waves each of which is oriented at a distinctive angle.

4.3 Multichannel Pattern Restoration System

The recording and addressing architecture of a multichannel pattern restoration system are shown in Fig. 8. A single plane wave is used for all the image storage process similar
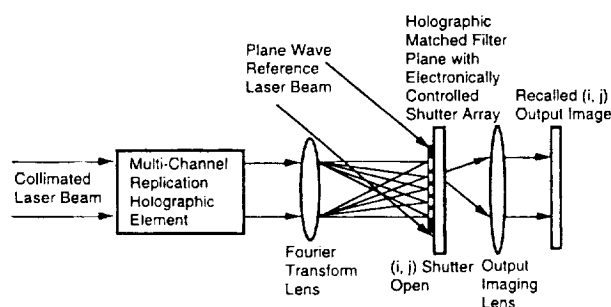
Fig. 8 Multichannel pattern restoration system addressing architecture.

Table 1 Desired SLM functional requirements.

Functional Features	Desired Specifications
Space-bandwidth product	1042 × 1042
Aperture dimensions (mm×mm)	5 × 5
Speed (frames/s)	1000
Dynamic range	100:1
Light efficiency	90%
Cost	$100 or less

to that of Fig. 6(a). In the image restoration process, the object beam is shut off and the (i,j)'th stored object image can be restored by using the same reference beam and electronically controlled selection shutters placed in front of the output imaging lens. The image stored at the (i,j)'th matched filter position will be holographically retrieved by the recording reference beam. In this case, only one image at each filter can be stored and recalled. The inverse Fourier transform is performed by the lens placed after the matched filter array. The restored image can be displaced at its focal plane.

5 Discussion

The definition and functional requirements for a traditional RAM have been realized electronically with impressive accomplishments and on-going progress in capacity, speed, and compactness. The optical RAM described in this paper is not intended to compete with the digital electronic RAM. The optical RAM architecture can offer an unique feature in high-speed parallel optical pattern recognition over an extremely large database. However, to achieve the special-purpose computing goals, technological advancement and breakthroughs in some of the key optical components are required. The challenges and opportunities in the research and development of the components are now briefly discussed.

5.1 Laser Sources

It is desired to have a laser source comparable to a laser diode in size with a power level comparable to that of an argon ion laser. However, the laser diodes have very poor coherent length and are not suitable for making holograms. The diode-pumped solid state laser has high power output but also lacks of coherence. Hence at the present time it is necessary to use large-frame lasers as recording sources.

5.2 SLMs for Data Input

The SLM for the input in the optical RAM poses a challenge for device technology development. Many kinds of SLMs have been developed. These include the Hughes liquid crystal light valve, the microchannel plate SLM, the microdeflection mirror SLM, the ferroelectric liquid crystal SLM, and the liquid crystal television SLM. For high-speed optical RAM operation, high-frame-rate SLMs with high dynamic range, small size, and large numbers of pixels are required. The desired functional requirements for the SLM are listed in Table 1.

No single currently available SLM has all the desired features, and the price of high-quality SLMs is too high to

use to construct a practical optical RAM. The liquid crystal television SLM is the only inexpensive SLM that meets the low-cost requirement, but it has other limitations including speed, contrast, and resolution.

5.3 Optical Lenses and Mirrors

To achieve optimum light utilization efficiency, Fourier optical lenses and mirrors must be specifically designed and fabricated. Ideally, a miniaturized optical system with an input lens of an effective aperture of less than 5×5 mm and with other components designed based on this aperture is desired.

5.4 Shutter Arrays

A single-aperture mechanical shutter can be used to write the input data into the memory. Mechanical shutters have an aperture of 100% transmittance. The position of the shutter can be precisely translated under the control of a PC. An alternative method is to use a liquid crystal shutter array. These shutters are available mostly in reflection mode with high distinction ratios. In the addressing mode, the shutters can be completely removed and hence will not affect the performance of the memory retrieval or pattern recognition functions.

5.5 Holographic Recording Materials

Candidates for real-time holographic recording materials include nonlinear photorefractive crystals, photopolymers, and thermoplastic materials. The recording sensitivity of the thermoplastic material is comparable to that of silver halide film. A simple and compact charging system must be developed for the thermoplastic recording device. More sensitive photorefractive and photopolymer materials must be developed for large-capacity memory.

5.6 Output Detectors

Photodiodes can be used for the detection of a single output signal. An array of output signals can be detected by a CCD array. Large-array position determinable smart pixel devices are required for pattern classification applications.

5.7 Light Budget Estimate, Speed, and Applications

Next, we make an estimate of the light budget for a two-stage HORAM based on realizable optical components. Assume a laser power of 5 W is used. The collimating optics reduces its power by a factor of 70%, the input SLM reduces its power by a factor of 90%, the Dammann grating by 80%, the hololens by 50%, and each of the shutter arrays by 50%. Since part of the beam is used by the reference beam, another factor of 90% will be multiplied, miscellaneous light loss of the components is represented by a factor of 70%. The overall factor is the multiplication of all the factors. The resulting factor is about 4%. By dividing the resulting light power by 2000, a maximum of 100 μW is available for the recording of a single matched filter. The same power level is available for retrieval. If the matched filter has a 50% diffraction efficiency, the correlation signal has an output of at most 50 μW, which is sufficient for the detection devices. Based on this estimate, the power levels will reach its limit if we have a 10,000-channel HORAM.
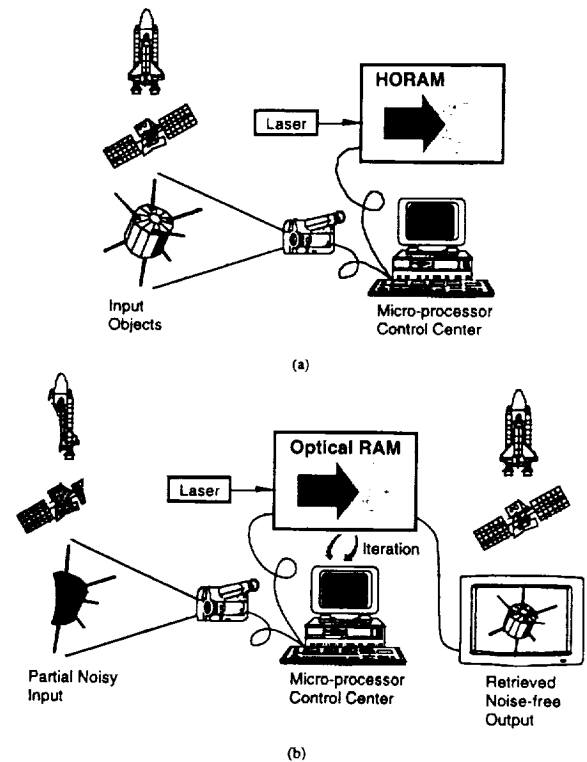
Fig. 9 Examples of HORAM applications: (a) memory process and (b) information retrieval.

The retrieval and processing speed is limited by that of the input SLM. For a 10,000-channel HORAM, if all the optimum values of the parameters are used and we assume that the speed the input SLM is 1000 frames/s with 400 $\times$ 600 binary pixels, the processing speed is estimated to be 240 Gbits/s. This speed for pattern recognition is valuable for certain specific applications.

With respect to the applications of these specific optical computing methods, one example of these applications is illustrated in Fig. 9. Figure 9(a) shows how memorization is accomplished in the HORAM by placing the objects as represented by the satellite and space shuttle in the view of a video camera. Over tens of thousands of 2-D data can be stored. Microprocessors can be used to control the random access to any data set from the memory. After the HORAM memorizes all the images presented to it, it becomes smart. When an input such as a partial and noisy space shuttle, as shown in Fig. 9(b), is presented to it, the HORAM can recover and display at the output screen the perfectly retrieved image. In addition, the HORAM can be used to recognize an input and tells us whether it belongs to the memory. For example, if the fingerprints of FBI's most wanted criminals are stored in the memory, the HORAM can determine whether an arbitrary input fingerprint belongs to one of the criminals. The recognition can be accomplished remotely and the HORAM can make a decision at the speed of light!

6 Conclusions

We have described a new technique of using multiple stages of free-space interconnection holographic elements

to implement a HORAM. We have demonstrated the technique with a memory capacity of over 2000 images. Potentially, seemingly limited only by the laser power, tens of thousands of images can be stored. Microprocessors can be used to control the random access to any data set from the memory. Each of the thousands of Fourier transforms in the array can be used to record a matched filter of an input image. Simultaneous optical pattern recognition and/or data processing of the superlarge array means a computing speed of the order of at least 10^{11} bits/s. This speed is faster than those obtainable by any other methods reported. For example, if the fingerprints of FBI's most wanted criminals are stored in the memory, the HORAM can determine whether an arbitrary input fingerprint belongs to one of the criminals. The recognition can be accomplished remotely and the HORAM can make the decision at the speed of light!

Acknowledgments

References

1. B. J. Goertzen and P. A. Mitkas, "Volume holographic storage for large relational databases," *Opt. Eng.* 35(7), 1847–1853 (1996).
2. P. B. Berra, A. Ghafoor, P. A. Mitkas, S. J. Marcinkowski, and M. Guizani, "The impact of optics on data and knowledge base systems," *IEEE Trans. Knowl. Data Eng.* 11, 111–132 (1989).
3. N. V. Kukhtarev, V. B. Markov, S. G. Odulov, M. S. Soskin, and V. L. Vinetskii, "Holographic storage in electrooptic crystals, I. Steady state," *Ferroelectrics* 22, 949–964 (1979).
4. J. F. Heanue, M. C. Bashaw, and L. Hesselink, "Volume holographic storage and retrieval of digital data," *Science* 265(5173), 749–752 (1994).
5. F. H. Mok, "Angle-multiplexed storage of 5000 holograms in lithium niobate," *Opt. Lett.* 18, 915–917 (1993).
6. S. Yin, H. Zhou, F. Zhao, M. Wen, Z. Yang, and F. T. S. Yu, "Wavelength multiplexed holographic storage in a sensitive photorefractive crystal using a visible light tunable diode laser," *Opt. Commun.* 101, 317–321 (1993).
7. P. A. Mitkas and L. J. Irakliotis, "Three-dimensional optical storage for database processing," *J. Opt. Mem. Neural Net.* 3(2), 87–98 (1994).
8. J. H. Hong, I. McMichael, T. Y. Chang, W. Christian, and E. G. Paek, "Volume holographic memory systems: techniques and architectures," *Opt. Eng.* 34(8), 2193–2203 (1995).
9. D. Psaltis, "Parallel optical memories," *Byte* 17(9), 179–182 (1992).
10. J. R. Wullert II and Y. Lu, "Limits of capacity and density of holographic storage," *Appl. Opt.* 33(11), 3192–3196 (1994).
11. F. T. S. Yu and S. Yin, "Thick volume photorefractive crystal wavelength-multiplexed reflection-type matched filter," *Opt. Mem. Neural Net.* 3, 207–214 (1994).
12. D. Gregory, G. Duthie, and H. K. Liu, "Large memory real-time multichannel multiplexed pattern recognition," *Appl. Opt.* 23, 4560–4570 (1984).
13. H. K. Liu, J. Barhen, and N. Farhat, "Unipolar terminal-attractor based neural associative memory with adaptive threshold," U.S. Patent No 5,544,280 (Aug. 1996).
14. H. K. Liu and J. Wu, "Optical implementations of terminal-attractor based associative memory," *Appl. Opt.* 31 4631–4644 (1992).
15. H. K. Liu and T. H. Chao, "Liquid crystal television spatial light modulators," *Appl. Opt.* 28, 4772–4780 (1989).
16. H. Dammann and K. Grotler, "High-efficiency in-line multiple imaging by means of multiple phase holograms," *Opt. Commun.* 3, 312–315 (1971).
17. M. Blume, F. B. McCormick, P. J. Marchand, and S. C. Esener, "Array interconnect systems based on lenslets and CGH," *Proc. SPIE* 2537, 180–193 (1995).
18. Y. Z. Liang, D. Z. Zhao, and H. K. Liu, "Multifocus dichromated gelatin hololens," *Appl. Opt.* 22, 3451–3459 (1983).
19. J. W. Goodman, *Introduction to Fourier Optics*, McGraw-Hill, New York (1968).

Hua-Kuang Liu is a professor of electrical engineering at the University of South Alabama (USA) and a Distinguished Visiting Scientist at the Center for Engineering Systems Advanced Research of the Oak Ridge National Laboratory. Before joining USA in September 1995, Dr. Liu was a senior research scientist with the Jet Propulsion Laboratory (JPL), California Institute of Technology. He received his PhD degree in electrical engineering from Johns Hopkins University. Dr. Liu was a professor of electrical engineering at the University of Alabama from 1969 to 1984, has presented many invited talks, seminars, and short courses at national and international meetings and universities, and was a record holder as the three-time recipient of the Best Faculty Research Award awarded by the Capstone Engineering Society in the years 1979, 1982, and 1984. In research, Dr. Liu has managed and directed major R&D projects sponsored by National Aeronautics and Space Administration (NASA), Department of Defense, and Department of Energy agencies and industries. He has been a group leader of advanced optoelectronic computing and information processing R&D groups at JPL. Dr. Liu's research specialties include optoelectronic computing, high-volume data storage and random access memory, information processing, and neural networks. During the last decade, Dr. Liu has acquired and managed contracts and projects totaling over $7 million. In new technology development, he holds over 27 U.S. patents and NASA Awards and Certificates of Recognition for Technology Innovation. He was recognized by the Caltech Patent Office as the most prominent inventor in modern optics in the history of NASA/JPL. Dr. Liu has published more than 200 technical papers, has participated in many university committees, has organized and chaired over 30 national and international conferences, and has served as a referee for archival journals and as a reviewer for major funding agencies. In 1975, Dr. Liu founded a high-tech firm, Lumin Inc., which has made many important cutting edge technology discoveries. Dr. Liu is a fellow of the OSA and SPIE and is listed in several national and international Who's Who publications.

Yahong Jin received her PhD degree in physics from the Rensselaer Polytechnic Institute, Troy, New York, and her BS and MS degrees from Shanghai Jiao Tong University, Shanghai, China. Since 1995, she has been a visiting assistant professor of electrical engineering at the University of South Alabama, Mobile. From 1994 to 1995, she was a visiting scientist at the Advanced Optoelectronic Computing Laboratory of the Jet Propulsion Laboratory, California Institute of Technology, Pasadena, working on optical information processing, pattern recognition, and holography. Her current research interests include optoelectronic computing and holography, ultrafast electromagnetic switching and optical communications, nonlinear crystals, and optical memory and data storage. Dr. Jin has published over 20 refereed journal papers and one book chapter and has made over 20 presentations at national and international conferences. She is a member of the IEEE, the American Physical Society, and SPIE.

Neville I. Marzwell is project manager for advanced concepts and technology innovation at the Jet Propulsion Laboratory (JPL), California Institute of Technology, Pasadena, and has 25 years experience in defense and aerospace systems technologies in which he initiated various technology innovations. His area of expertise is large optical systems for imaging far fainted objects and high energy lasers. He has developed adaptive, distributive, and hierarchical control systems for large space structures and has contributed developments in autonomous space systems, robotics, and teleoperated systems. Before joining JPL, he was program manager of advanced technology with the High Energy Laser Research at the Rockedyne Division of Rockwell International, where he developed innovative wavefront sensing and correction systems and optical and sensor protection systems for surveillance satellites. At Honeywell Research Center he was instrumental in advances in IR detector technology, electro-optical materials, and fiber optical systems. Dr. Marzwell was a Josephine de Karman fellow at the California Institute of Technology and holds a PhD in applied physics and materials science from Caltech. He has published 55 papers in refereed and professional journal and has served on various national and international panels and workshop, conferences, and symposium committees.